ADVANCED ELECTRONIC MATERIALS Open Access
www.advelectronicmat.de

Materials, Device Structures, and Applications of Flexible Perovskite Light-Emitting Diodes

Jae Hong Jang, Shi Li, Dae-Hyeong Kim, Jiwoong Yang,* and Moon Kee Choi**

The flexible type of displays, which can alter their shape freely (e.g., bendable or foldable displays) according to situational demands, is under an intense spotlight due to applications in human-friendly mobile electronics. Among various types of light-emitting diodes (LEDs), meanwhile, perovskite-based LEDs (PeLEDs) have garnered particular attention in recent years as next-generation optoelectronic devices due to their exceptional optical characteristics, such as high efficiency (up to theoretical limits), high color purity, wide color gamut over the entire visible range, and ultrathin form factor. By integrating perovskite materials on an ultrathin flexible substrate with a proper encapsulation layer, the flexible PeLEDs, which can conform to various curved surfaces and be stably operated in an ambient condition, have been developed. Here, recent advances of the flexible PeLEDs are reviewed. First, light-emitting materials and device structures for the PeLEDs are introduced. Then, research progress on the flexible PeLEDs, either with and without the encapsulation layer are summarized. Next, some representative application examples of the flexible PeLEDs are briefly discussed. Finally, this review includes a brief discussion on future prospects.

1. Introduction

Since their first manufacture in 1960s, light-emitting diodes (LEDs) have been placed in a key position of the display market due to their distinctive electrical and optical advantages, such as high brightness, low power consumption, and long lifetime. Accordingly, as an effort to improve the light-emitting performance, LEDs based on various light-emitting materials have been intensively researched, including those based on organic materials,[1–3] quantum dots,[4–8] and perovskites.[9–12] Among them, perovskite-based LEDs (PeLEDs) have received significant attention due to their exceptional optical characteristics: high photoluminescence quantum yield (PLQY; ≈100%),[13] high absorption coefficient,[14,15] uniform emission wavelength regardless of size uniformity, and extraordinary color purity (full-width at half-maximum (FWHM) < 20 nm).[16,17] Such vivid color expression and high optoelectronic performance are based on the shallow traps located inside the valence band (VB) and conduction band (CB) of the perovskite materials.[18]

Meanwhile, there has been increasing demand of flexible displays for mobile phones, monitors, and televisions owing to their increased portability, multicasting, and space-saving capabilities (**Figure 1**). After the first flexible organic LED was reported by Heeger group in 1992,[19] various types of flexible displays[20–22] have been launched on the display market. In the early stage, curved monitors, curved smartphones, and wearable fitness trackers with

J. H. Jang, M. K. Choi
Department of Materials Science and Engineering
Ulsan National Institute of Science and Technology (UNIST)
Ulsan 44919, Republic of Korea
E-mail: mkchoi@unist.ac.kr

S. Li, J. Yang
Department of Energy Science and Engineering
Daegu Gyeongbuk Institute of Science and Technology (DGIST)
Daegu 42988, Republic of Korea
E-mail: jiwoongyang@dgist.ac.kr

D.-H. Kim
School of Chemical and Biological Engineering
Institute of Chemical Processes
Seoul National University
Seoul 08826, Republic of Korea
E-mail: dkim98@snu.ac.kr

D.-H. Kim, M. K. Choi
Center for Nanoparticle Research
Institute for Basic Science (IBS)
Seoul 08826, Republic of Korea

J. Yang
Energy Science and Engineering Research Center
Daegu Gyeongbuk Institute of Science and Technology (DGIST)
Daegu 42988, Republic of Korea

M. K. Choi
Graduate School of Semiconductor Materials and Devices Engineering
Center for Future Semiconductor Technology (FUST)
Ulsan National Institute of Science and Technology (UNIST)
Ulsan 44919, Republic of Korea

The ORCID identification number(s) for the author(s) of this article can be found under https://doi.org/10.1002/aelm.202201271

DOI: 10.1002/aelm.202201271

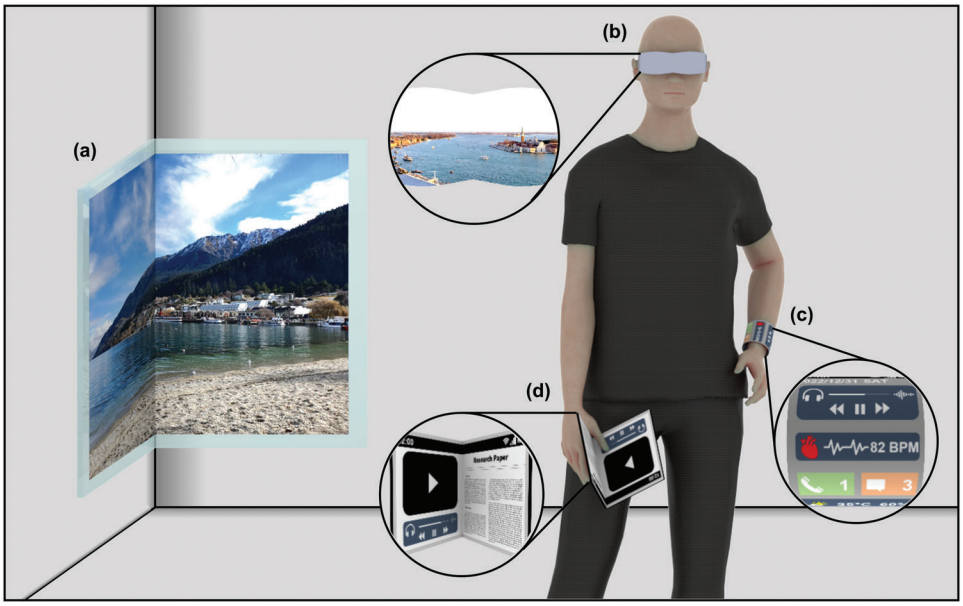

Figure 1. Schematic illustration of future application of PeLEDs. a) Flexible TV and monitor, b) XR device, c) flexible smartwatch, and d) foldable portable device.

curved displays were developed to provide wide field-of-view, extra user interfaces, and enhanced wearability, respectively. The curved monitors can offer outstanding immersion and visual comfort by maintaining the identical distance between the eyes and the display in any angles while reducing light reflection.[23] The wearable trackers, which are curved to fit the wrist curvature, improve comfort even for long-term wearing and measure biological signals accurately. Recently, foldable-display-based smartphones (Samsung electronics, 2019) and 65 in. rollable TVs (LG Electronics, 2020) were also commercialized, which can change their shape according to the user's intent and provide wide screens without space restrictions. A curvature-tunable monitor (LG Electronics, 2022) was also commercialized to offer realistic visual information to users. However, these displays still have limitations in terms of the degree of deformation (uniaxial bending and/or rolling) and the bending radius. For achieving high deformability, displays must be sufficiently thin to avoid high tensile and compression stresses.[24,25] To replace thick and rigid substrates, flexible substrates with micrometer-level thickness have been suggested, such as polyethylene terephthalate (PET), polyimide (PI), polyethylene naphthalate (PEN), polydimethylsiloxane (PDMS), NOA, and parylene.[26–31] Introducing an appropriate encapsulation layer is also essential for placing the display in the neutral mechanical plane of the entire device to increase the operational stability.[32]

Here, we review recent advances in the flexible type of PeLEDs, particularly focusing on the material development and device designs. First, we review the detailed strategies for designing materials and devices to fabricate highly efficient PeLEDs, which is a crucial prerequisite for creating flexible PeLEDs. Then, we summarize recent progress in the research on flexible PeLEDs with and without encapsulation layer. Finally, we briefly discuss various applications of flexible PeLEDs and conclude this review with a brief discussion on prospects, providing a comprehensive overview of the state-of-the-art developments in flexible PeLEDs and their potential impact on the emerging field of flexible electronics.

2. Perovskite-Based Light-Emitting Layers

In general, the efficiency of LEDs can be estimated by measuring their external quantum efficiency (EQE), which is defined as the ratio of the number of photons emitted by the LED to the number of injected electrons. The EQE can be expressed by Equation (1)[24]

$$\mathrm{EQE} = \frac{\#\ \text{of emitted photons}}{\#\ \text{of the supplied electorns}} = \gamma \times \chi \times \eta_{\mathrm{PL}} \times \eta_{\mathrm{oc}} \tag{1}$$

where γ is the fraction of injected electrons that form excitons, χ is the ratio of excitons with spin-allowed optical transitions, η_{PL} is the PLQY of the light-emitting materials, and η_{PL} is the outcoupling efficiency. Because the EQE of LEDs is typically proportional to the PLQY of the light-emitting layers, the development of perovskite-emitting layers with high PLQY is an important prerequisite for realizing high-performance PeLEDs. Many important strategies, including compositional engineering (e.g., A-site cations, B-site cations, and X-site anions)[33–35] and dimensional engineering (e.g., 2D/quasi-2D, 1D, and 0D perovskites),[36–38] have been proposed to increase the EQE by decreasing the nonradiative recombination. In this section, we discuss the design strategy of perovskite materials for the development of highly efficient PeLEDs.

2.1. Compositional Engineering of Perovskite Materials

Figure 2a displays the perovskite crystal structure with the general chemical formula of ABX_3. Basically, the A cations are in

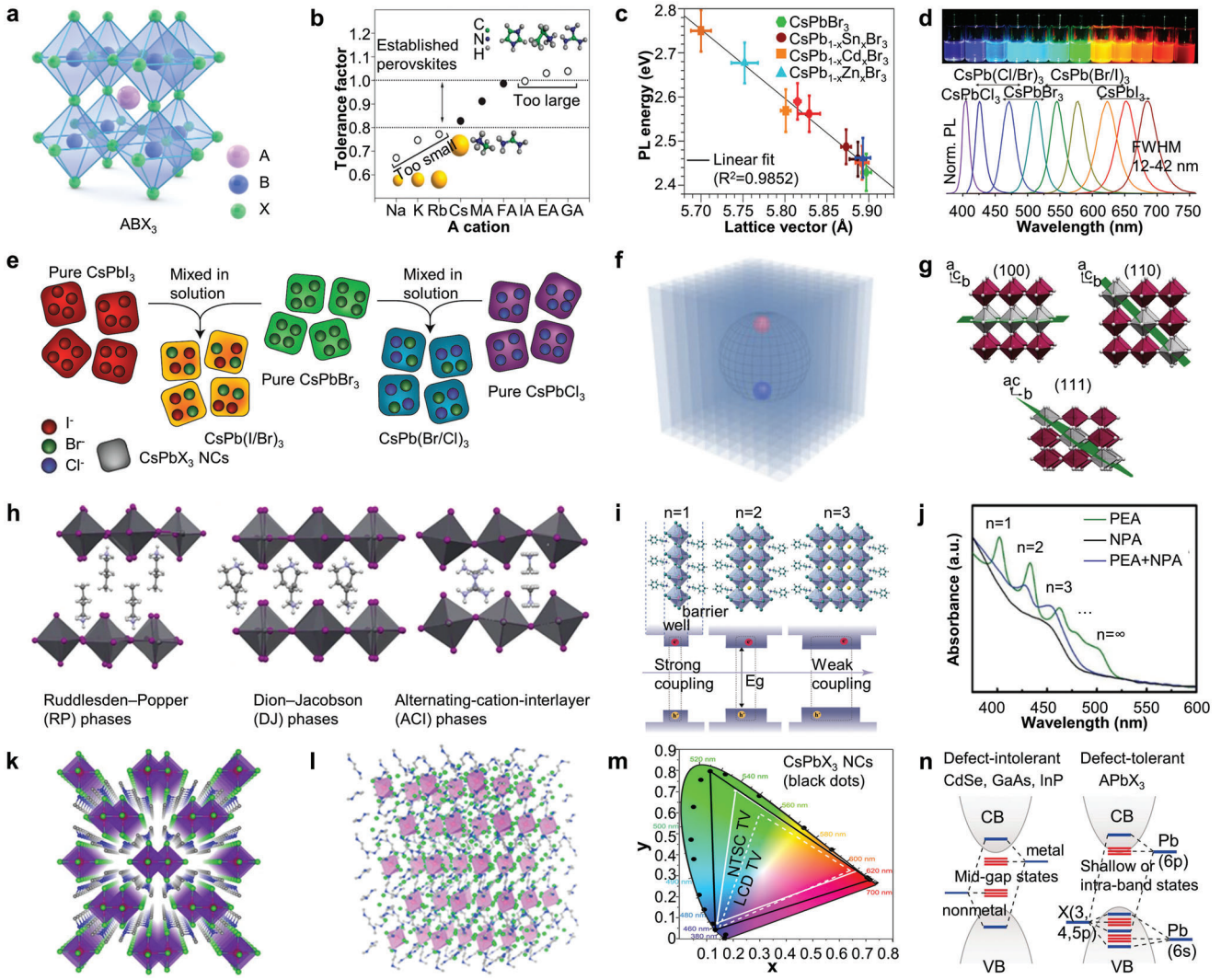

Figure 2. Perovskite light-emitting layers. a) Representative crystal structure of perovskites. b) Tolerance factor of $APbI_3$ perovskites with various cations in the A-site. Reproduced with permission.[47] Copyright 2019, American Chemical Society. c) PL energy as a function of the lattice vector in M (M = Sn^{2+}, Cd^{2+}, and Zn^{2+}) doped $CsPb_{1-x}M_xBr_3$ NCs. Reproduced with permission.[55] Copyright 2017, American Chemical Society. d) Colloidal $CsPbX_3$ (X = Cl^-, Br^-, I^-, or mixed $Cl^-/Br^-/I^-$) NCs with emission wavelength tunability from 410 to 700 nm by adjusting the composition in the X-site (bottom); corresponding photographs of $CsPbX_3$ solutions in toluene under UV irradiation (λ = 365 nm) (top). Reproduced with permission.[57] Copyright 2015, American Chemical Society. e) Schematic of $CsPbX_3$ NCs with bandgaps tunable by halide anion exchange. Reproduced with permission.[58] Copyright 2015, American Chemical Society. f) Schematic representation of 3D bulk perovskites with weak exciton binding energy. Reproduced with permission.[60] Copyright 2022, Springer Nature. g) Derivation of 2D/quasi-2D perovskites by cutting crystal planes of 3D perovskites: (100), (110), and (111). Reproduced with permission.[66] Copyright 2018, American Chemical Society. h) Schematic of crystal structures of (100)-oriented 2D/quasi-2D perovskites. Reproduced with permission.[75] Copyright 2022, Springer Nature. i) Schematic crystal structures of 2D/quasi-2D perovskites with various *n* values and the corresponding electronic band structures determined by quantum and dielectric confinement effects. Reproduced with permission.[85] Copyright 2021, Springer Nature. j) Absorption spectra of quasi-2D $CsPbBr_3$ with different ligands. Reproduced with permission.[90] Copyright 2020, Wiley-VCH GmbH. k) Schematic of the crystal structure of 1D perovskites. Reproduced with permission.[91] Copyright 2017, Springer Nature. l) Schematic of the crystal structure of 0D perovskites. Reproduced with permission.[88] Copyright 2021, Wiley-VCH GmbH. m) Representative Commission Internationale de l'Eclairage (CIE) diagram showing the coordinates of $CsPbX_3$ (X = Cl^-, Br^-, I^-, or mixed $Cl^-/Br^-/I^-$) NCs and compared to common color standards (LCD TV: dashed white triangle, NTSC TV: solid white triangle). Reproduced with permission.[57] Copyright 2015, American Chemical Society. n) Schematic of the electronic band structure of typical defect-intolerant semiconductors (e.g., CdSe, GaAs, and InP) (left) and defect-tolerant halide perovskite (e.g., $APbX_3$) (right). Reproduced with permission.[104] Copyright 2017, The American Association for the Advancement of Science.

12-fold cuboctahedral coordination and the B cations are in six-fold octahedral coordination, surrounded by X anions. The metal cations at the B site coordinate with the X anions to form a regular octahedral $[BX_6]^{4-}$ structure, with A-site cations occupying the gap of the octahedron, which are interconnected by common vertices to form a continuous 3D network structure.[39] By changing the elemental species in the perovskite materials, the optical/electrical properties and stability of perovskites can be significantly tuned, which suggests their great potential of high material tenability for device applications.[40–42] In addition, owing to the

high defect tolerance of perovskite materials, various elements can be selected and applied at different sites to obtain various perovskite materials with controlled optical properties.[43]

The crystal structure of perovskites is sensitive to the ionic radius of the A-site cations because of the limitation of the octahedral $[BX_6]^{4-}$ framework, which can greatly affect the stability of perovskites.[44,45] To evaluate the stability of the perovskite structure, the Goldschmidt tolerance factor (t) was proposed, as shown in Equation (2)[46]

$$t = \frac{r_A + r_X}{\sqrt{2}\left(r_B + r_X\right)} \tag{2}$$

where r_A, r_B, and r_X are the ionic radii of the A-, B-, and X-site cations, respectively. In general, stable perovskites with ideal cubic structures can be obtained for $0.9 < t < 1.10$, while tetragonal and orthorhombic structures form for $0.81 < t < 0.9$.

Figure 2b summarizes the changes in the tolerance factors according to the various cations in the A site.[47] Representative A-site cations that can yield stable perovskite structures include Cs^+, MA^+, and FA^+. Smaller inorganic cations such as Na^+, Ka^+, and Rb^+ can deform and eventually destroy the crystal structure. Organic cations with larger ionic radii (e.g., imidazolium (IA^+), ethylamine (EA^+), and guanidinium (GA^+)) cannot enter the octahedral gap, promoting the growth of octahedral $[BX_6]^{4-}$ along the in-plane direction. This can induce the formation of periodic 2D/quasi-2D perovskite sheets interconnected by corner-sharing halide anions. 2D/quasi-2D perovskites are discussed in Section 2.2.

In addition, the bandgap of perovskite materials heavily depends on the choice of A-site cations. A-site cations with different ionic radii in the octahedral space cause contraction or expansion of the crystal lattice of perovskites owing to the tilt of the inorganic octahedron, thereby changing the bond length and angle of the B–X bonds.[48–50] In general, increasing the size of the A-site cations results in a red shift in the absorption of the perovskites. A-site cation compositional engineering provides a solution for fabricating perovskites with a wider bandgap tunability range when halide composition engineering is ineffective. For example, because the Goldschmidt tolerance factor of $FAPbI_3$ is close to the limit for stable perovskite structures, adjusting the bandgap of perovskites using halide anions further reduces the stability of perovskites. Conversely, using A-site cations with smaller ionic radii can alleviate the Goldschmidt tolerance factor while obtaining perovskites with tunable bandgaps.

In addition to A-site cations, B-site cations play an important role in the stability of perovskites. The selection of B-site cations should not only satisfy the Goldschmidt tolerance factor (t) range but also satisfy the requirement of the octahedral factor (μ)

$$\mu = \frac{R_B}{R_X} \tag{3}$$

Typical 3D perovskites have $0.442 \leq \mu \leq 0.895$.[51] The B-site cations located at the center of the octahedron not only affect the crystal phase of perovskites by changing the degree of octahedral rotation or tilt but also determine their electronic level and emission properties.[52] For perovskites, the orbital contribution of octahedrons $[BX_4]^{6-}$ mainly determines the band structure near the band edge (i.e., VBM and CBM), which is directly related to their band gaps.[53] The bond angle and bond length of B–X have important effects on the bandgap of perovskites, which can be adjusted by changing the cations in the B-sites.[54] For example, Stam et al. reported M (M = Sn^{2+}, Cd^{2+}, and Zn^{2+})-doped $CsPbBr_3$ nanocrystals (NCs) through post-synthetic cation exchange reactions (Figure 2c).[55] The Pb^{2+} cations are partially replaced by M^{2+} cations with a smaller ionic radius, which shortens the Pb–Br bond length. This causes a blue shift in the absorption and emission spectra, which is linearly related to lattice contraction. Surprisingly, M-doped $CsPbBr_3$ NCs preserve the high PLQY (>50%) with narrow bandwidth (FWHM: ≈80 meV), which is comparable to undoped $CsPbBr_3$ NCs.

Lastly, X-site anions also directly affect the optical properties of perovskites because of their difference in electronegativity.[56] The bond length of the B–X bonds decreases with a decrease in the ionic radii of the halide anions, which leads to the enhancement of the interaction between the halide anions and the B-site cations, and weakens the absorption ability of the perovskites at longer wavelengths. Therefore, tuning the ratio between Cl^-, Br^-, and I^- ions is a straightforward strategy to achieve continuously tunable light emission of perovskite materials. For example, Kovalenko et al. synthesized all-inorganic $CsPbX_3$ (X = Cl^-, Br^-, I^-, or mixed $Cl^-/Br^-/I^-$) NCs with a size of 4–15 nm, demonstrating tunable light emission covering the entire visible spectra from 410 to 700 nm by simply changing the composition of halide ions (Figure 2d).[57] Based on similar principles, halide anion exchange reactions have been widely used to control the halide ion content in perovskites, which has driven the development of mixed halide perovskites (Figure 2e).[58]

2.2. Dimensional Engineering of Perovskite Materials

The small exciton binding energy in 3D bulk perovskite structures (e.g., $MAPbBr_3$, 84 meV)[59] leads to a low probability of radiative recombination (Figure 2f).[60,61] In low-dimensional perovskites, including 2D/quasi-2D,[62] 1D,[63] and 0D perovskites, the exciton binding energy of low-dimensional perovskites is higher than that of their bulk counterparts because of quantum confinement effects.[64] Consequently, low-dimensional perovskites exhibit outstanding optical and electrical characteristics, which make them promising for LED applications.

2D/quasi-2D perovskites are derived from 3D perovskites truncated along specific crystal planes (e.g., (100), (110), or (111) crystal planes) and maintained by introducing bulky organic aliphatic or aromatic cations into the A site of the perovskites to isolate the inorganic layers (Figure 2g).[44,65,66] Typical (100)-oriented 2D/quasi-2D perovskites have the general formula of $A'_2A_{n-1}B_nX_{3n+1}$ ($1 \leq n < \infty$), where A' is generally a larger organic cation between inorganic layers, A is a smaller monovalent cation incorporated into the inorganic framework, B is a divalent metal cation, X is a halide ion, and n represents the number of inorganic layers between insulating organic layers. The (110)-oriented 2D/quasi-2D perovskite have the general formula of $A'_2A_mB_mX_{3m+2}$ ($1 \leq m < \infty$). Due to the highly distorted

octahedrons, few cations can stabilize them and there are many interesting physical phenomena, such as self-trapped excitons,[67,68] and broadband/white light emission at room temperature.[69] The (111)-oriented 2D/quasi-2D perovskite have the general formula of $A'_2A_{q-1}B_qX_{3q+3}$ ($q > 1$). Since some metal sites need to be eliminated when cutting along the volume diagonal of perovskite cell, (111)-oriented 2D/quasi-2D perovskite can only be formed from group 15 B^{3+} ions (e.g., As, Sb, Bi) by the introduction of B-site vacancies rather than large organic cations.[70] In this section, we focus on the most widely studied (100)-oriented 2D/quasi-2D perovskites.

The (100)-oriented 2D/quasi-2D perovskites can be further divided into Ruddlesden–Popper (RP) phases,[71,72] Dion–Jacobson (DJ) phases,[73,74] and alternating-cation-interlayer (ACI) phases (Figure 2h).[75] The general formulas of RP-, DJ-, and ACI-phase 2D/quasi-2D perovskites are $A''_2A_{n-1}B_nX_{3n+1}$, $A''A_{n-1}B_nX_{3n+1}$, and $A''A_nB_nX_{3n+1}$ ($1 \leq n < \infty$), respectively, where A'' is interlayer "spacer" cation, where A'' in the RP phases is aryl ammonium or alkyl cation (e.g., phenylethylammonium (PEA^+), butylammonium (BA^+)), and in the DJ phases is divalent interlayer organic cations (e.g., 3-(aminomethyl)piperidinium (3AMP) and 4-(aminomethyl)piperidinium (4AMP)). Notably, GA^+ is the only A'' cation reported to form the ACI-phase 2D/quasi-2D perovskites. The inorganic layers in the RP phase usually show in-plane displacement with one octahedral unit (1/2, 1/2);[76] while adjacent layers in the DJ phase are stacked on top of each other without any displacement;[77] the ACI phase is in between, combining the layer stacking characteristics of the RP- and DJ-phase structures by adopting an A''-A alternating-cation arrangement in the interlayer place, which leads to an octahedral rotation and a (1/2, 0) displacement.[78,79] In addition, the interlayer distance of these three phases is quite different, which is directly influenced by the length of cations.[80] The interlayer distance of RP phase is the largest among the three phases due to the monovalent cationic bilayer structure;[81] that of DJ phase is smallest due to the divalent cationic monolayer structure; that of ACI phase is in between, which is granted by the compact stack of small cations.[15] Moreover, a weak van der Waals gap in RP phase forms between the cationic bilayer and two adjacent octahedral sheets;[82] there is no gap in DJ phase by forming hydrogen bonds through the two amino diamine compounds at both ends of adjacent layers, demonstrating DJ phase is the highest stability;[83] in the ACI phase, both hydrogen bonds and partial van der Waals gaps are present.[84]

2D/quasi-2D perovskites have natural quantum well structures, in which inorganic layers as quantum wells and organic layers with a lower dielectric constant act as quantum barriers (Figure 2i).[85,86] Excitons can be effectively confined in quantum wells owing to the large difference in permittivity.[87] The width of the quantum well shortens as the number of inorganic layers decreases, which results in an increase in the excitonic binding energy (up to 300–400 meV) with a quantum confinement effect.[88,89] High exciton binding energies can lead to strong radiative recombination. The n values of 2D/quasi-2D perovskites are influenced by various long-chain organic cations. Jin et al. demonstrated blue 2D/quasi-2D $PEA_2NPA_1Cs_2Pb_3Br_{12}$ PeLEDs with $n = 2$ and 3 through the synergistic effect of dual ligands (benzeneethanamine, hydrobromide; PEABr, and *N*-(2-bromoethyl)-1,3-propanediamine dihydrobromide; $NPABr_2$) (Figure 2j).[90] PEA^+ increases the PLQY of perovskite films with different n numbers (from $n = 1$ to $n = \infty$), while NPA^{2+} helps narrow the phase distribution of perovskites ($n = 2$ and 3).

1D perovskites can be obtained by further cutting 2D/quasi-2D perovskites into metal halide wires. The chain-like $[BX_6]^{4-}$ octahedrons by corner-sharing, edge-sharing, or face-sharing are surrounded by large organic cations (Figure 2k).[91] Different from 3D bulk and 2D/quasi-2D perovsiktes, 1D perovskites, with self-trapped excited states formation and large structural distortions, exhibit broadband emissions with large Stokes-shift of ≈1 eV due to the stronger quantum confinement and exciton–lattice interaction.[92–95] Based on this theory, Yuan et al. synthesized a novel 1D core–shell $C_4N_2H_{14}PbBr_4$ perovskite quantum wires with self-trapped excited states, in which edge-sharing octahedral $[PbBr_4]^{2-}$ chains as the core are surrounded by the organic cations $C_4N_2H_{14}{}^{2+}$ as the shell, achieving broadband bluish white-light emissions (FWHM = 157 nm at 475 nm).[22] Therefore, 1D perovskite is a highly promising single-component white-light-emitting material.

The 0D perovskite is composed of isolated $[BX_6]^{4-}$ octahedrons or metal halide clusters separated by organic or inorganic cations, and the remaining 3D-like structures are independent of each other owing to strong interactions between the $[BX_6]^{4-}$ octahedra (Figure 2l).[88,96,97] The generated excitons are confined in isolated octahedra, which results in a large bandgap due to reduced orbital overlap, thus maximizing the potential for exciton recombination.[98] The optical properties of most 0D perovskites depend on isolated octahedra or clusters because of the weak electronic coupling caused by large organic or inorganic cations. In addition to tuning the optical properties of perovskites by their composition and size, the fabrication of core–shell structures can provide additional flexibility for designing 0D perovskites.[99,100]

The discussed compositional and dimensional flexibility endow perovskites with unique properties, such as a wide range of color tunability and high color purity, making them promising for the next-generation display applications (Figure 2m).[101,102] For example, halide perovskites exhibit narrower PL and fine-tuning of emission peaks through compositional and dimensional engineering, which allows for a wider color gamut, compared to the current standard of conventional liquid crystal display (LCD) TV and the National Television Standard Committee (NTSC) specification. Furthermore, unlike conventional semiconductor materials, in which defects act as trap states between the VB and CB, these orbitals in perovskites are located inside or near the VB and CB (Figure 2n).[103–105] This makes perovskite highly defect tolerable, which is advantageous for LED applications. These benefits are particularly enhanced for flexible LEDs that must withstand various mechanical deformations.

3. Perovskite-Based LEDs

According to Equation (1), a high PLQY of perovskite materials cannot ensure a high EQE of PeLEDs. For example, an imbalance in charge injection, interface loss, and other factors can decrease the EQE of PeLEDs.[106–110] Therefore, the design and selection of the device structures play an essential role in the development of high-performance PeLEDs. In this section, we discuss recent advances in PeLEDs including device structures, light emission mechanisms, and charge transport layer materials.

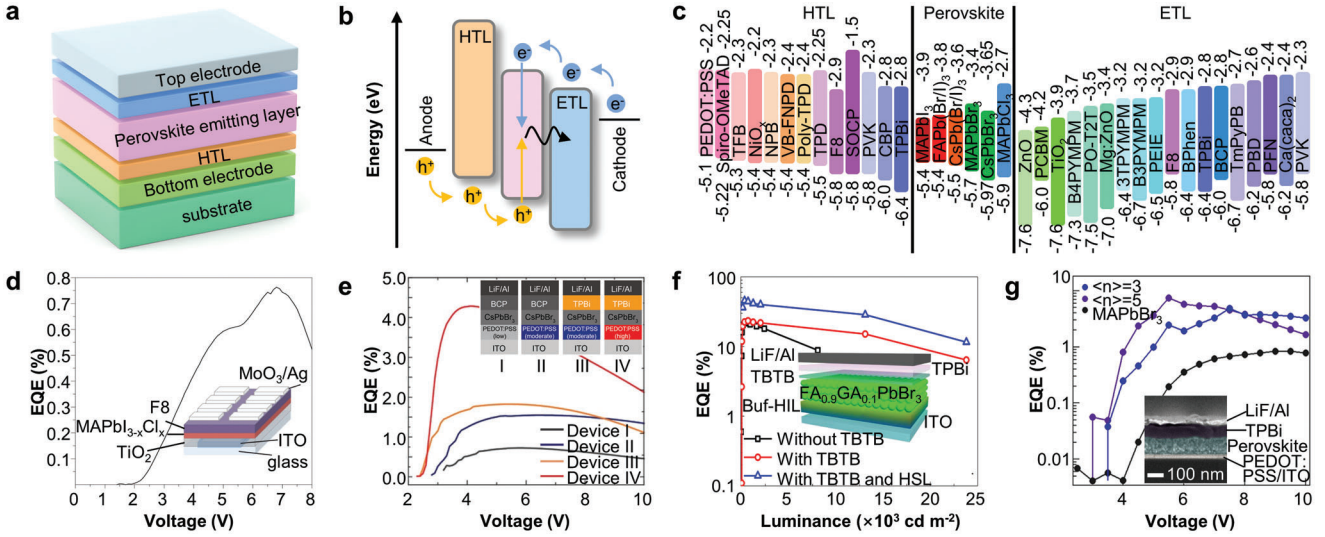

Figure 3. Perovskite-based LEDs. a) Typical device structure, and b) light emission mechanism of PeLEDs. c) Energy level alignment of various materials used as HTLs, perovskites, and ETLs in the PeLEDs. d) EQE–*V* characteristics of near-infrared $MAPbI_{3-x}Cl_x$ PeLEDs modified with Al_2O_3. The inset is the corresponding device architecture. Reproduced with permission.[9] Copyright 2014, Springer Nature. e) EQE–*V* characteristics of green $CsPbBr_3$ PeLEDs fabricated with various ETL and HTL materials. The insets are the corresponding device architectures. Reproduced with permission.[113] Copyright 2016, Wiley-VCH GmbH. f) EQE–*L* characteristics of $FA_{0.9}GA_{0.1}PbBr_3$ NCs PeLEDs with or without a TBTB interlayer. The inset is the device structure of PeLEDs with the TBTB interlayer. Reproduced with permission.[116] Copyright 2021, Springer Nature. g) EQE–*V* characteristics of quasi-2D $PEA_2(MA)_{n-1}Pb_nBr_{3n+1}$ PeLEDs with different *n* values. The inset is the cross-sectional SEM image of PeLED devices. Reproduced with permission.[118] Copyright 2017, American Chemical Society.

3.1. Device Structure and Light Emission Mechanism of PeLEDs

Typical PeLEDs consist of a substrate, top/bottom electrodes (anode and cathode), carrier transport layers (e.g., electron transport layer (ETL) and hole transport layer (HTL)), and a light-emitting layer based on perovskites (**Figure 3**a). The perovskite light-emitting layer is sandwiched between an n-type ETL and a p-type HTL to form a multilayer heterojunction architecture for better charge injection and confinement of injected charges in the perovskites, resulting in enhanced light emission. According to the position of the charge transport layers, the structure of PeLEDs can be divided into conventional bottom-emitting (HTL-perovskite-ETL) devices and inverted top-emitting (ETL-perovskite-HTL) devices.

Figure 3b shows the light-emission mechanism of the PeLEDs. The externally applied electrons are injected into the CB of the perovskite through the cathode and ETL, while externally applied holes are injected into the VB of the perovskite through the anode and HTL. Subsequently, the injected electrons and holes are confined in the perovskite emitting layer. In the perovskite layer, photons are generated by the radiative recombination of the injected electron–hole pairs and emitted to the outside of the PeLED, whose energy (wavelength) is determined by the bandgap of the perovskite layer. More device examples and electroluminescence (EL) properties will be discussed in the following section.

3.2. EL Characteristics of PeLEDs

The charge transport layers, which control the injection of charge carriers into perovskites, are key components of the high-performance PeLED. Figure 3c summarizes the energy levels of materials commonly used in PeLED devices, including perovskites, ETLs, and HTLs. ETL materials are commonly composed of n-type materials, whereas HTL materials are widely composed of p-type materials. Because the electron mobility of ETLs is usually higher than the hole mobility of HTLs, PeLEDs suffer from unbalanced charge injection. The ideal charge transport layers require the following factors: i) the energy level of the charge transport layers should match that of perovskites to minimize the charge injection potential barrier and decrease the quenching of carriers at the interface while blocking the reverse carrier transport. ii) The charge mobilities of the HTL and ETL materials should be similar. iii) The preparation method of the charge transport layers should be compatible with perovskites (e.g., solvent orthogonality), which should not damage the perovskite materials during processing.[111]

As a notable example, Tan et al. reported bright PeLEDs with $MAPbI_{3-x}Cl_x$, $MAPbBr_3$, and $MAPbBr_2I$ emissive layers to achieve near-infrared (NIR), green, and red emissions, respectively, working in air at room temperature (Figure 3d).[9] Owing to the different energy levels of the three perovskite materials, various charge-transport layers were chosen for more efficient charge injection and confinement in the perovskite layers. In the NIR PeLEDs, 25 nm titanium dioxide (TiO_2) prepared by atomic layer deposition was used as an ETL as well as a hole-blocking layer, and poly(9,9'-dioctylfluorene) (F8) acted as an HTL and electron-blocking layer. An ultrathin (1 nm) alumina layer was sandwiched between the TiO_2 and perovskite layers to prevent luminescence quenching at the TiO_2/perovskite interface. In this configuration, the NIR LED had an EQE of 0.76% and an internal quantum efficiency (IQE) of 3.4%. In green and red LEDs, poly(3,4-ethylenedioxythiophene):polystyrene sulfonate (PEDOT:PSS) was employed as an HTL, while F8 was

employed as an ETL, resulting in high-performance green LEDs with an EQE of 0.1% and IQE of 0.4%, and red LEDs with an EQE of 0.018%.

However, the low hole mobility of conventional hole transport layers can lead to unbalanced injection of electrons and holes. The excess electrons are often trapped at perovskite/ETL interfaces by various defects, reducing the electron–hole radiative recombination efficiency.[112] To solve this issue, charge-transport layers with similar charge mobilities have been used. Ling et al. fabricated solution-processed green $CsPbBr_3$ PeLEDs with sandwiched structures (Figure 3e).[113] A poly(ethylene oxide) (PEO)-based additive was spin-coated to obtain smooth (roughness of 9 nm) and pinhole-free $CsPbBr_3$-PEO films with a PLQY of 60% and uniform current distribution. The low electrical/optical performance of PeLEDs, which is caused by the low conductivity of PEO additives, can be improved by optimizing the charge transport layers. PEDOT:PSS (hole mobility: >5.55 $\times 10^{-5}$ cm^2 V^{-1} s^{-1})[114] and (2,2',2''-(1,3,5-benzinetriyl)-*tris*(1-phenyl-1-*H*-benzimidazole)) (TPBi) (electron mobility: 8×10^{-5} cm^2 V^{-1} s^{-1}) were employed as an HTL and an ETL, respectively, for balancing electron and hole injection efficiencies. All-inorganic-material-based PeLEDs with optimized injection efficiencies achieved an EL performance of 53 525 cd m^{-2} and EQE of 4.26%.

In addition, the introduction of interlayers is regarded as an effective approach for balancing charge injection efficiencies.[115] Kim et al. reported zero-dipole guanidinium cation (GA^+)-doped $FAPbBr_3$ NC-based PeLEDs with interlayer engineering (Figure 3f).[116] Because of the limited bulk solubility of GA^+ cations in perovskites, GA^+ cations with more hydrogen bonds are located in the crystals and surfaces of smaller perovskites, creating an entropy-stabilized phase and stabilizing the undercoordinated sites. In addition, a 5 nm insulating 1,3,5-*tris*(bromomethyl)-2,4,6-triethylbenzene (TBTB) interlayer was sandwiched between the perovskite and TPBi layers as a healing agent of bromide vacancies, which can passivate halide vacancy defects in perovskites and improve the charge balance in PeLEDs by retarding electron injection into the perovskite layer. The optimized PeLEDs with the indium tin oxide (ITO)/Buf-HIL/$FA_{0.9}GA_{0.1}PbBr_3$/TBTB/TPBi/LiF/Al structure exhibited an EQE of 45.5% and a current efficiency (CE) of 203 cd A^{-1}.

Interestingly, quasi-2D perovskites have been shown to possess spontaneous band gradients and have been successfully applied to PeLEDs.[117] Sargent group developed a dimension-tunable quasi-2D $PEA_2(MA)_{n-1}Pb_nBr_{3n+1}$ (phenylethylammonium, PEA^+) PeLED with an energy-funneled structure (Figure 3g).[118] The dimensions of the quasi-2D perovskite were tuned by changing the ratio of methylammonium iodide to phenylethylammonium iodide. The perovskite containing a series of different quantum-sized grains exhibited a high PLQY of 60%. This is attributed to the inhomogenous energy distribution, which is beneficial for funneling energy into grains with a lower bandgap. By tailoring the energy landscape in quasi-2D perovskites, green PeLEDs exhibited an EQE of 7.4% with a high brightness of 8400 cd m^{-2}.

Recently, Lee group reported highly efficient and stable green PeLEDs using a in situ reaction of benzylphosphonic acid (BPA) with 3D polycrystalline perovskite films.[119] The BPA split large 3D perovskites into PeNCs by fabricating PeNC/BPA core/shell

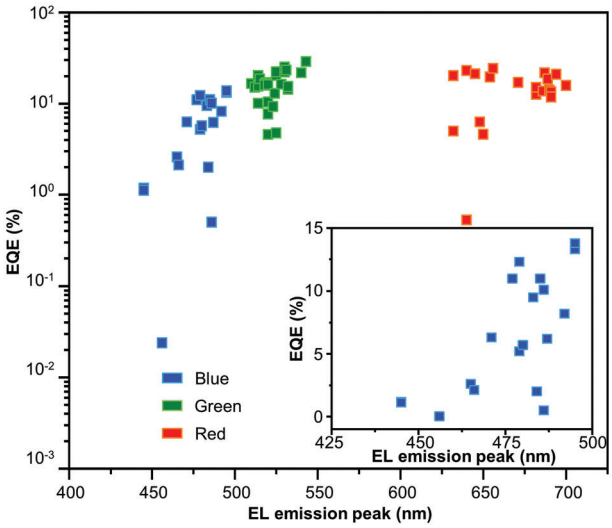

Figure 4. Research development and the representative achievements of blue, green, and red PeLEDs (blue squares, green squares, and red squares correspond to blue, green, and red PeLEDs, respectively). Details of each point are shown in Tables 1–3.

structures. The covalent bonding between BPA and Pb atom in PeNCs decreased the trap density while keeping the high charge transport property of 3D perovskites. PeLEDs fabricated with core/shell PeNCs exhibited maximum luminance of 470 000 cd m^{-2}, maximum EQE of 28.9%, and half-lifetime of 520 h at 1000 cd m^{-2}.

Researchers have achieved great success in improving the performance of PeLEDs through material composition engineering, dimensional engineering, and device structure optimization (**Figure 4**, **Table 1**,[108,120–137] **Table 2**,[107,119,11,99,138–160] and **Table 3**[120,150,35,161–176]), which serve as a fundamental prerequisite for developing flexible PeLEDs. Currently, the EQE of NIR, red, and green PeLEDs exceed 20%, which is close to that of the best quantum dot LEDs and organic LEDs. However, the efficiency of blue PeLEDs is significantly lower than that of red and green PeLEDs. Blue light is one of the most important components of the three primary colors, and it plays a vital role in full-color displays and white lighting. Size control and hybrid halogen engineering are the most widely used approaches for realizing blue PeLEDs.[126,177] However, the low solubility of chemicals used for Cl precursors makes it difficult to prepare high-quality blue-emitting perovskite films. Ion migration induced by vacancy defects leads to the phase segregation of perovskites, resulting in the generation of trap centers, thereby reducing the efficiency and stability of blue PeLEDs. The larger bandgap of blue perovskites leads to a larger barrier for carrier injection, which makes it difficult to use conventional charge-transport layers used in green or red LEDs, causing great challenges toward efficient charge injection.

4. Flexible PeLEDs without Encapsulation

Compared with traditional rigid PeLEDs, flexible PeLEDs have a wider range of potential applications in wearable and portable devices owing to their unique advantages, such as flexibility and

Table 1. Details of blue perovskite LEDs in Figure 4.

Device structure	Perovskite structure	EL peak emission [nm]	EQE [%]	Ref.
ITO/NiO_x/PVK/perovskite/TPBi/LiF/Al	NCs	445	1.18	[120]
ITO/NiO/$Cs_3Cu_2I_5$/TPBi/LiF/Al	NCs	445	1.12	[121]
ITO/PEDOT:PSS/PVK/2D $CH_3NH_3PbBr_3$/TPBi/LiF/Al	2D	456	0.024	[122]
ITO/PVK/PFI/PEA_2PbBr_4/(P2m2)/3TPYMB[a)]/Liq/Al	2D	465	2.6	[123]
ITO/TFB[b)]/PFI/$CsMn_yPb_{1-y}Br_xCl_{3-x}$/TPBi/LiF/Al	NCs	466	2.12	[124]
ITO/TFB/PFI/$CsMn_yPb_{1-y}Br_xCl_{3-x}$/3TPYMB/Liq/Al	NCs	471	6.3	[125]
ITO/NiO/PVK/2D/3D perovskite/TPBi/LiF/Al	2D/3D	477	11	[126]
ITO/PEDOT:PSS/Poly-TPD/$PEA_2Cs_{1.6}MA_{0.4}Pb_3Br_{10}$/TPBi/LiF/Al	2D/3D	479	5.2	[127]
ITO/PEDOT:PSS-PTAA[c)]/$CsPbBr_3$-$CsPbBr_3$/TPBi/LiF/Al	NCs	479	12.3	[128]
ITO/PEDOT:PSS/$CsPbCl_{0.9}Br_{2.1}$-PEABr/TPBi/LiF/Al	2D/3D	480	5.7	[129]
ITO/NiO/TFB/2D $CH_3NH_3PbBr_3$/TPBi/LiF/Al	2D/3D NCs	483	9.5	[130]
ITO/LiF/(Cs/Rb/FA/PEA/K)$Pb(Cl/Br)_3$/LiF/Bphen[d)]/LiF/Al	3D	484	2.01	[131]
ITO/PEDOT:PSS/$CsPbBr_3$:PEACl/TPBi/LiF/Al	2D/3D	485	11	[132]
ITO/NiO(or TFB/PFI)/$CsPbBr_xCl_{3-x}$/TPBi/LiF/Al	NCs	486	0.5	[133]
ITO/PVK/$PEA_xPA_{2-x}(CsPbBr_3)_{n-1}PbBr_4$/TPBi/LiF/Al	2D/3D	486	10.11	[134]
ITO/PEDOT:PSS/PVK/$BA_2Cs_{n-1}Pb_n(Br/Y)_{3n+1}$/TPBi/LiF/Al	2D/3D	487	6.2	[108]
ITO/(PVK):(F4-TCNQ)[e)]/$(PEA)_{0.75}(GA)_{0.25}$/(TPPO)[f)]/TPBi/LiF/Al	2D/3D	492	8.2	[135]
ITO/m-PEDOT:PSS/$PEA_2(CsPbBr_3)_2PbBr_4$/TBPi/LiF/Al	2D/3D	495	13.3	[136]
ITO/PEDOT:PSS:PFI/PVK/Perovskite/TPBi/LiF/Al	NCs	495	13.8	[137]

[a)] 3TPYMB: *Tris*(2,4,6-trimethyl-3-(pyridin-3-yl)phenyl)borane [b)] TFB: Poly[(9,9-dioctylfluorenyl-2,7-diyl)-*co*-(4,4′-(*N*-(4-sec-butylphenyl)diphenylamine)] [c)] PTAA: Poly(triaryl amine), Poly[bis(4-phenyl)(2,4,6-trimethylphenyl)amine] [d)] Bphen: 4,7-Diphenyl-1,10-phenanthroline [e)] F4-TCNQ: 2,3,5,6-Tetrafluoro-7,7,8,8-tetracyano-quinodimethane [f)] TPPO: Triphenylphosphine monoxide.

light weight.[178] However, proper material choice and integration should be done to maximize the device performance even on the flexible substrates. Since the flexibility of the device is highly dependent on its thickness, it is important to control the thickness of each component. In PeLEDs, the thicknesses of charge transport layers, emission layer, and electrodes are tens of nanometer scale while the thickness of the polymeric substrate tends to measure in the range of tens to hundreds of micrometers. Furthermore, the inorganic transparent electrodes, such as ITO, exhibit a high Young's modulus and may fracture readily under external strain. Hence, engineering the thickness and modulus of the polymeric substrate and the development of a flexible, transparent electrode are critical components to achieve high-performance flexible PeLEDs. In this section, representative examples of commonly used flexible substrates and electrodes for the flexible PeLEDs will be reviewed (**Table 4**).[139,179–202]

4.1. Flexible Substrates

Flexible substrates for deformable PeLEDs need to meet several key requirements, such as high optical transparency, good oxygen/moisture barrier properties, and excellent material properties for various mechanical deformations. Polymers, such as PET, PI, PEN, and polyurethane (PU) have been widely used as substrates for flexible PeLEDs.[186,193,196,203,204]

Wang et al. used a PDMS/PET substrate to develop flexible inkjet-printed $MAPbBr_3$ LEDs (**Figure 5**a).[205] The highly scalable inkjet-printing process can produce smooth and pinhole-free films with a patterning resolution of 250 µm while greatly reducing the fabrication time (≈25 min per device). The all-inkjet-printed PeLED exhibited a novel four-layer structure without separate charge transport layers, including PEO-modified PEDOT:PSS as a bottom electrode, a $MAPbBr_3$/PEO composite film as an emitting layer, a poly(ethylene imine) (PEI) buffer layer, and a AgNW network as a top electrode. The PEI buffer layer protects the perovskite crystals from being damaged by the mixed solvents (isopropanol and ethylene glycol) of the AgNW ink, reduces the electron injection barrier, and enhances the interfacial adhesion between the AgNW network and the perovskite layer. The PeLED device maintained excellent mechanical stability even after 5000 bending cycles with a radius of curvature of 2.5 mm (Figure 5b).

Colorless PI can endure higher temperatures (>200 °C), which can allow more severe fabrication processes. Zhao et al. developed red $MAPbI_3$ PeLEDs on flexible PI/AgNW substrates (Figure 5c).[184] The AgNW ink with TiO_2 gel was embedded into a colorless PI substrate to obtain ultrasmooth (roughness of 0.7 nm), highly transparent (>85%), and highly conductive (25 Ω sq^{-1}) flexible electrodes. To enhance the mechanical robustness and efficiency of perovskites, 4-fluorobenzylammonium iodide (FPMAI) was selected as a bulky organo-ammonium halide additive to fabricate flexible PeLEDs, obtaining a high EQE of 13%. The efficient PeLED with FPMAI showed excellent robustness, including no EQE degradation after 1000 cycles of bending at a bending radius of 2 mm and only a 20% loss in EQE at a bending radius of 1 mm (Figure 5d).

Optically active polymers are commonly used as flexible substrates of PeLEDs.[206] Lu et al. fabricated highly flexible $CsPbI_3$ nanocrystal PeLEDs on a photopolymer (NOA63)-based flexible substrate using a smooth Ag film as the cathode (Figure 5e).[190]

Table 2. Details of green perovskite LEDs in Figure 4.

Device structure	Perovskite structure	EL peak emission [nm]	EQE [%]	Ref.
ITO/NiO_x/PVK/perovskite/TPBi/LiF/Al	2D	510	16.6	[138]
ITO/PEDOT:PSS/PVK/$CsPbBr_3$/TPBi/Liq/Al	NCs	512	15.17	[99]
ITO/ZnO/PEDOT:PSS/PVK/$CsPbBr_3$/TPBi/LiF/Al	NCs	514	20.3	[107]
ITO/PEDOT:PSS/$CsPbBr_3$/perovskite/TPBi/LiF/Al	NCs	514	10.1	[139]
ITO/PEDOT:PSS/PTAA/$PEA_2Cs_{n-1}Pb_nBr_{3n+1}$/TPBi/LiF/Al	2D	514	15.5	[140]
ITO/PEDOT:PSS/PTAA/$CsPbBr_3$/TPBi/LiF/Al	NCs	515	18.7	[141]
ITO/PEDOT:PSS/$CsPbBr_3$/TPBI/LiF/Al (Trifluoroacetate additive)	3D	519	17	[142]
ITO/PEDOT:PSS/PTAA/$CsPbBr_3$/TPBi/LiF/Al ($ZnBr_2$ additive)	NCs	518	16.48	[143]
ITO/TFB/PVK/$Na_2Cs_{n-1}Pb_nBr_{3n+1}$/TPBi/LiF/Al	2D/3D	518	15.9	[144]
ITO/NiO_x/TFB/PVK/$CsPbBr_3$/TPBi/LiF/Al	3D	520	16.2	[145]
ITO/ZnO/PVP[a]/$Cs_{0.87}MA_{0.13}PbBr_3$/CBP[b]/MoO_3/Al	3D	520	10.4	[146]
ITO/PEDOT:PSS/PolyTPD/$CsPbX_3$/TPBi/LiF/Al	NCs	520	4.59	[147]
ITO/PEDOT:PSS/TFB/PolyTPD/PVK/$CsPbBr_3$/TPBi/LiF/Al	2D/3D	520	7.7	[148]
ITO/a-ZSO/$CsPbBr_3$/NPD[c]/MoO_x/Ag	3D	523	9.3	[149]
ITO/PEDOT:PSS/PolyTPD/$MAPbX_3$/B3PYMPM[d]/Cs_2CO_3/Al	NCs	524	12.9	[150]
ITO/PEDOT:PSS/$CsPbBr_3$-MABr/B3PYMPM/LiF/Al	3D	525	20.3	[11]
ITO/PEDOT:PSS/$CsPbX_3$/TPBi/LiF/Al	3D	525	4.76	[151]
ITO/PEDOT:PSS/$FPEA_2MA_{n-1}Pb_nBr_{3n+1}$/TmPyPB[e]/LiF/Al	2D/3D	525	20.36	[152]
ITO/$NiMgLiO_x$/Perovskite/B3PYMPM/LiF/Al	Quasi-2D	525	22.29	[153]
ITO/PEDOT:PSS/TFB/$FAPbBr_3$/TPBi/LiF/Al	NCs	528	16.3	[154]
ITO/PVK/Perovskite/TPBi/LiF/Al	Quasi-2D	≈530	22.2	[155]
ITO/PVK/Modified perovskite/TPBi/LiF/Al	Quasi-2D	530	25.1	[156]
ITO/PEDOT:PSS/PFI/$FA_{1-x}GA_xPbBr_3$/TBTB/TPBi/LiF/Al (defect passivation)	NCs	531	23.4	[157]
ITO/PEDOT:PSS/$PEA_2(FAPbBr_3)_{n-1}PbBr_4$/TPBi/LiF/Al	2D/3D	532	14.36	[158]
ITO/PEDOT:PSS:PSS-Na/$PEA_2(FAPbBr_3)_2PbBr_4$/TOPO[f]/TPBi/LiF/Al	Quasi-2D	532	15.4	[159]
SOCP[g]/$MAPbBr_3$/TPBi/LiF/Al	3D	540	21.8	[160]
FTO/GraHIL/In situ core/shell perovskite/ZADN[h]/LiF/Al	NCs	543	28.9	[119]

[a] PVP: Polyvinylpyrrolidone [b] CBP: 4,4′-Bis(*N*-carbazolyl)-1,1′-biphenyl [c] NPD: *N*,*N*′-Bis(naphthalen-1-yl)-*N*,*N*′-bis(phenyl)-2,2′-dimethylbenzidine [d] B3PYMPM: 4,6-Bis(3,5-di(pyridin-3-yl)phenyl)-2-methylpyrimidine, 4,6-Bis(3,5-di-3-pyridinylphenyl)-2-methylpyrimidine [e] TmPyPB: 1,3,5-Tri(m-pyridin-3-ylphenyl)benzene [f] TOPO: trioctylphosphine oxide [g] SOCP: self-organized conducting polymer [h] ZADN: 2-[4-(9,10-Di-naphthalen-2-yl-anthracen-2-yl)-phenyl]-1-phenyl-1*H*-benzoimidazole.

The adhesion between the cured photopolymer and thermally evaporated Ag was better than that between Ag and the Si substrate, ensuring ultrathin (80 nm) and ultrasmooth (roughness of 0.6 nm) Ag films to attach to the photopolymer using template-stripping technology. This results in enhanced electron injection and reduces the probability of a short circuit. Semitransparent MoO_3/Au was used as the top electrode to improve the transparency of the whole device. Furthermore, the robust PeLED showed no significant change in the EL performance and morphology (i.e., no cracks and dark spots) after 1000 times of repeated bending cycles with 180° bending (Figure 5f).

4.2. Flexible Electrodes

High visual transparency (>90% light transmission), low sheet resistance (<100 Ω sq^{-1}), and notable mechanical compatibility for deformation are key requirements of the flexible and transparent electrodes in flexible optoelectronic devices. Thin ITO on polymer substrates is currently one of the most extensively used transparent electrodes for flexible LEDs. Due to the inherent brittleness of ITO electrodes, however, their stress-tolerance is limited. Hence, alternative materials, including silver nanowires (AgNWs), graphene, conductive polymers, and MXenes, have been thoroughly investigated to substitute fragile ITO electrodes, thereby enhancing the flexibility of resultant devices.[207–209]

AgNWs are the most commonly used 1D nanomaterials for flexible electrodes.[194,210–212] Unfortunately, the contact resistance of AgNWs dramatically increases during the mechanical deformation of the electrode by slipping or even breaking the internanowire contacts. Therefore, AgNW composites have been extensively explored for the development of highly flexible PeLEDs. In this context, Zhao et al. fabricated colloidal $MAPbBr_3$ NC-based flexible PeLEDs composed of AgNW-polymer composite electrodes with ultralow surface roughness (<1 nm), low sheet resistance of 10 Ω sq^{-1}, and high transmittance of 86% at 550 nm (Figure 5g).[181] Poly-(*N*-vinyl carbazole):4,4′-cyclohexylidenebis[*N*,*N*-bis(4-methylphenyl)benzenamine] (PVK:TAPC) was chosen as the HTL to improve both hole transport and injection efficiency. Compared with polycrystalline perovskite films, perovskite NC films showed enhanced mechanical durability in the repeated

Table 3. Details of red perovskite LEDs in Figure 4.

Device structure	Perovskite structure	EL peak emission [nm]	EQE [%]	Ref.
ITO/PEDOT:PSS/PEA_2SnI_4/TPBi/LiF/Al	2D/3D	632	5	[161]
ITO/PEDOT:PSS/Poly-TPD/$MAPbI_XBr_{3-X}$/TPBi/LiF/Al	NCs	632	20.28	[162]
ITO/PEDOT:PSS/PVK/$CH_3NH_3PbBr_xI_{3-x}$/TPBi/LiF/Al	NCs	640	0.53	[120]
ITO/PEDOT:PSS:PFI/Perovskite/TPBi/LiF/Al	QD	640	23	[163]
ITO/PEDOT:PSS/Poly-TPD/$(CsPbBr/I)_3$/TPBi/LiF/Al	NCs	645	21.3	[35]
ITO/ZnO/PEI/$CsPb(Br/I)_3$/CBP/TCTA[a]/MoO_3/Au	NCs	648	6.3	[164]
ITO/a-ZSO/$CsPbBr_3$/NPD/MoO_x/Ag	NCs	650	4.6	[150]
ITO/PEDOT:PSS/PTAA/PVK/Perovskite/TPBi/LiF/Al	NC	654	19.6	[165]
ITO/PEDOT/Poly-TPD/Perovskite/CNT2T[b]/LiF/Al	NC	≈656	24.4	[166]
ITO/ZnO/PEIE[c]/Perovskite/TFB/MoO_3/Au	3D	671	17.03	[167]
ITO/PEDOT:PSS/Poly-TPD/KI/Perovskite/TPBi/LiF/Al	NC	687	21.8	[168]
ITO/ZnO/PEI/$CsPbI_3$/TCTA/MoO_3/Au	NCs	682	12.6	[169]
ITO/ZnO/PEI/$CsPb_{0.64}Zn_{0.36}I_3$/TCTA/MoO_3/Au	NCs	682	15.1	[170]
Si/Ag/ZnO/PEI/$CsPbI_3$/TCTA/MoO_3/Au	NCs	686	13.7	[171]
ITO/Poly-TPD/$CsPbI_{2.8}Br_{0.2}$/TPBi/LiF/Al	2D/3D	689	18.6	[172]
ITO/PEDOT:PSS/Poly-TPD/$CsPbX_3$/TPBi/LiF/Al	NCs	690	14.08	[122]
ITO/ZnO/PEI/$CsPbI_{3-0.1}$/TCTA/MoO_3/Ag	NCs	691	13.5	[173]
ITO/ZnO/PEI/$CsPbI_3$/TCTA/MoO_3/Au	NCs	691	11.8	[174]
ITO/poly-TPD/$FA_{0.33}Cs_{0.67}Pb(I_{0.7}Br_{0.3})_3$/TPBi/LiF/Al (FPMATFA as an additive)	3D	694	20.9	[175]
ITO/ZnO/PEI/$FA_{0.87}Cs_{0.13}PbI_3$/CBP/MoO_3/Au	3D	700	15.8	[176]

[a] TCTA: *Tris*(4-carbazoyl-9-ylphenyl)amine [b] CNT2T: 3′,3‴,3⁗′-(1,3,5-triazine-2,4,6-triyl)*tris*([1,1′-biphenyl]-3-carbonitrile) [c] PEIE: polyethyleneimine.

bending tests, which was attributed to their ultrathin thickness. Owing to the mechanical robustness of the AgNW-polymer composite electrode and NCs layer, the PeLEDs could withstand 1000 cycles of bending at a radius of curvature of 4 mm without significant degradation (Figure 5h).

2D graphene is another excellent choice for flexible transparent electrodes owing to its outstanding electrical and physical properties.[213,214] Seo et al. developed a p-type four-layer graphene anode (4LG) to replace conventional ITO electrodes for $MAPbBr_3$-based flexible PeLEDs (Figure 5i).[182] The 4LG film was fabricated by repeated transfer of single-layer graphene grown by chemical vapor deposition. To improve the electrical conductivity of the 4LG film, HNO_3 vapor was used as a p-type dopant, decreasing sheet resistance from 225.7 ± 6.0 to 84.2 ± 2.7 Ω sq^{-1}. A self-organized gradient buffer hole injection layer (Buf-HIL) composed of a perfluorinated ionomer (PFI) was introduced between the 4LG film and $MAPbBr_3$ layers. The gradually increasing work function (from 5.2 to 5.95 eV) of the Buf-HIL layer overcomes the large hole injection potential barrier between graphene (4.4 eV) and $MAPbBr_3$ (5.9 eV). Compared to PeLEDs based on the ITO electrode, PeLEDs based on 4LG showed only ≈19% loss in performance after 1200 bending cycles (Figure 5j). Notably, metal-free graphene eliminates the formation of metal-induced nonradiative recombination of excitons in the emission layer, further improving the stability of the devices. Therefore, graphene anode-based PeLEDs exhibited excellent device performance (CE = 18.0 cd A^{-1}; EQE = 3.8%).

Conductive polymers are a promising candidate for flexible transparent electrodes in optoelectronic devices. Among the various conductive polymers, PEDOT:PSS has received considerable attention due to its exceptional properties, including high transparency, excellent conductivity, high deformability, and adjustable work function through the addition of dopants.[215–217] Jeong et al. reported PeLEDs incorporating a work function tunable anode (AnoHIL) based on PEDOT:PSS, which serves as both an anode and a hole injection layer.[216] The addition of tetrafluoroethylene-perfluoro-3,6-dioxa-4-methyl-7-octenesulphonic acid copolymer and a polar organic additive to PEDOT:PSS enabled AnoHIL to exhibit work function tunability (ranging from 4.4 to 5.8 eV), high conductivity (up to 50 S cm^{-1}), and high transparency (>90%) in the entire visible region. Compared to PeLEDs based on bare PEDOT:PSS, those based on AnoHIL showed significantly improved EL performance, including a high CE (42.0 cd A^{-1}) and EQE (8.66%).

In recent studies, MXene, novel 2D material with high electrical conductivity (0.5–8 kΩ sq^{-1})[218] and tunable physicochemical structure, has been regarded as a potential material for transparent flexible electrodes. Cao et al. demonstrated efficient and robust flexible quasi-2D $FEA_2Cs_{n-1}Pb_nBr_{3n+1}$ (n = 1–6) PeLEDs with a mixed-dimensional MXene-based composite electrode composed of 0D Ag nanoparticles (AgNPs)/1D AgNWs/2D $Ti_3C_2T_x$ MXene/3D PEDOT:PSS (Figure 5k).[200] MXene enables the quinoid phase transformation of PEDOT:PSS to enhance the electrical/thermal conductivity of the composite electrode. PEDOT:PSS with potassium citrate as the HTL facilitated hole transport because of the low energy barrier for carrier injection into perovskites, promoted the coverage and crystallinity of the perovskite, and suppressed nonradiative recombination by passivating the halide vacancies of the perovskite layer. The PeLEDs based on the composite electrode demonstrated stable operation (≈90% of the initial EQE was retained) after 500 bending cycles (Figure 5l).

Table 4. Recent advances in flexible PeLEDs.

Device structure	FWHM [nm]	CE [cd A^{-1}]	EQE [%]	Luminance [cd m^{-2}]	Minimum bending radius [mm]	Ref.
PET/ITO/PEDOT:PSS/$MAPbBr_3$:PEO/AgNWs/PU	18	–	–	1030	6	[179]
PDMS/PEDOT:PSS-PEO/$MAPbBr_3$-PEO/EInGa	–	3.2	0.62	15 960	40%[a]	[180]
PET/AgNWs/PEDOT:PSS/PVK:TAPC/$CH_3NH_3PbBr_3$ QDs/TmPyPB/CsF/Al	21	10.4	2.6	6960	2.5	[181]
PET/graphene/Buf-HIL/$MAPbBr_3$/TPBi/LiF/Al	21	16.1	–	13 000	1.9	[182]
PET/ITO/PEDOT:PSS/Perovskite/Bphen/LiF/Al	–	0.44	0.148	212	–	[183]
PI/AgNWs/PEDOT:PSS/poly-TPD/Perovskite/TPBi/LiF/Al	–	–	13	–	2	[184]
PET/AgNWs/PEDOT:PSS/$CsPbBr_3$: PEG[a]:PEABr/TPBI/LiF/Al	18	31	10.1	–	1	[139]
NOA63/SU-8/MoO_3/Au/PEDOT:PSS/$MAPbBr_3$/TPBi/LiF/Al	–	3.3	–	11 270	5	[185]
PEN/ITO/PEDOT:PSS/$MAPbBr_3$/BCP/LiF/Al	21	0.17	–	676	–	[186]
PEN/ITO/LiF/$CsPbBr_3$:Cs_4PbBr_6/TPBi/NiO_x/Al	–	4.16	1.37	2012	1	[187]
VHB/PI/AgNWs/PEDOT:PSS/TAPC:PVK/Perovskite QDs/TPBi/CsF/Al	20	9.2	–	3187	20%[f]	[188]
NOA63/composite electrode/Zonyl-treated PEDOT:PSS/quasi-2D perovskite/TPBi/LiF/Al	21	17.9	3.98	1060	2.5	[189]
Photopolymer/Ag/ZnO/PEI/$CsPbI_3$/TCTA/MoO_3/Au	37	8.2	0.8	827	180°[g]	[190]
PET/ITO/PEDOT:PSS/$MAPbBr_3$:PEG/ZnO/SMF[b]	22	–	–	–	–	[191]
PET/ITO/ZnO/PEIE/$FAPbI_3$/poly-TPD/MoO_3/Al	41	~153	~1	–	–	[192]
PET/Ag-Ni core–shell NW/Buf-HIL/$FAPbBr_3$/TPBi/LiF/Al	–	44.0	9.67	1378.4	–	[193]
PET/AgNWs/ZnO/PEDOT:PSS/$CsPbBr_3$/TPBi/LiF/Al	–	75	24.5	–	3	[194]
PET/ITO/HAT-CN[c]/TAPC/$CsPbBr_3$/PO-T2T[d]/Liq/Al	20	10.3	–	17550	10	[195]
PEN/ITO/TB(MA)/quasi-2D perovskite/TPBi/LiF/Al	–	14.7	8.3	2967	–	[196]
PET/PEDOT:PSS/quasi-2D perovskite/TPBi/LiF/Al	21.4	47.1	–	8300	1	[197]
PET/ITO/Li-doped NiO_x/$CsPbBr_3$/TPBi/LiF/Al	20	–	–	–	45°[g]	[198]
PET/ITO/poly-TPD/$MAPbI_3$/TPBi/LiF/Al	–	–	7.1	–	–	[199]
Composite electrode/KCA[e]:PEDOT:PSS/$PEA_2Cs_{n-1}Pb_nBr_{3n+1}$/TPBi/LiF/Al	–	54.1	16.5	49 807	10	[200]
Parylene/epoxy/ITO/PEDOT:PSS/poly-TPD/$CsPbBr_3$/TPBi/LiF/Al/Parylene		–	6.2	1	0.25	[201]
PET/ITO/PEDOT:PSS:PFI/$CsPbBr_3$/TPBi/LiF/Al	18	28.17	6.18	17 795	4	[202]

[a] PEG: poly(ethylene glycol) [b] SMF: silver microflake [c] HAT-CN: Dipyrazino[2,3-*f*:2′,3′-*h*]quinoxaline-2,3,6,7,10,11-hexacarbonitrile [d] PO-T2T: 2,4,6-*tris*[3(diphenylphosphinyl)phenyl]-1,3,5-triazine [e] KCA: potassium citrate [f] Uniaxial strain [g] Bending degree.

5. Ultrathin Flexible PeLED Encapsulation

For the long-term use of PeLEDs as deformable optoelectronic devices, it is crucial to strengthen the bending stability during the mechanical deformations (e.g., bending, folding, and twisting). Employing a top-encapsulation layer is essential for minimizing applied strains on the devices and protecting the active layer from exposure to oxygen and moisture. During bending, the inner side of the film undergoes compression while the outside of the film undergoes tension. A neutral mechanical plane that does not experience bending stress exists between these two. For flexible devices, it is crucial to place the active layer of the PeLED in the neutral mechanical plane between the encapsulation layers to reduce exposure to strain-induced stress.[219] In addition, exposure to air containing oxygen and moisture is a major factor in the degradation of flexible PeLEDs.[220] Under ambient conditions, water molecules in the air initially hydrate the perovskite crystal structure, resulting in a monohydrate phase in the single crystal. Oxygen exposure also causes the oxidation of not only the perovskite layer, but also the organic layers of HTL and ETL, causing further degradation of the PeLEDs.[221]

When a flexible LED is bent under external strain, compressive stress and tensile stress act upon the bottom and top parts of the device, respectively (**Figure 6**a). Therefore, without top encapsulation, tensile stress is continuously applied to the active layer during deformation. However, by encapsulating the top side of the device with a layer whose thickness is similar to that of the bottom substrate, the active layer itself becomes situated at the neutral mechanical plane; this structure ensures that the active layer is less affected by stress even under continuous mechanical deformation.

Solvent orthogonality must be considered for the selection of an appropriate solvent for the encapsulation layer formation, as various types of solvents (e.g., water, aliphatic solvent, and aromatic solvents) are utilized during the PeLED fabrication. Therefore, solvent-free polymers (e.g., NOA and Ecoflex) or vapor-deposited polymers (e.g., parylene) are preferred for the encapsulation layer, and thus the underlying active layers are not damaged by the solvent used in the encapsulation layer.

From this perspective, Park et al. reported the improvement of the bending mechanical behavior of a thin perovskite layer by using a flexible polymer passivation.[222] For mechanical behavior measurements, they spin-coated 300 nm thick lead halide perovskite onto a flexible polyethersulfone substrate and encapsulated it with two different polymer encapsulation layers, PEDOT:PSS and polystyrene (PS); these two polymers were

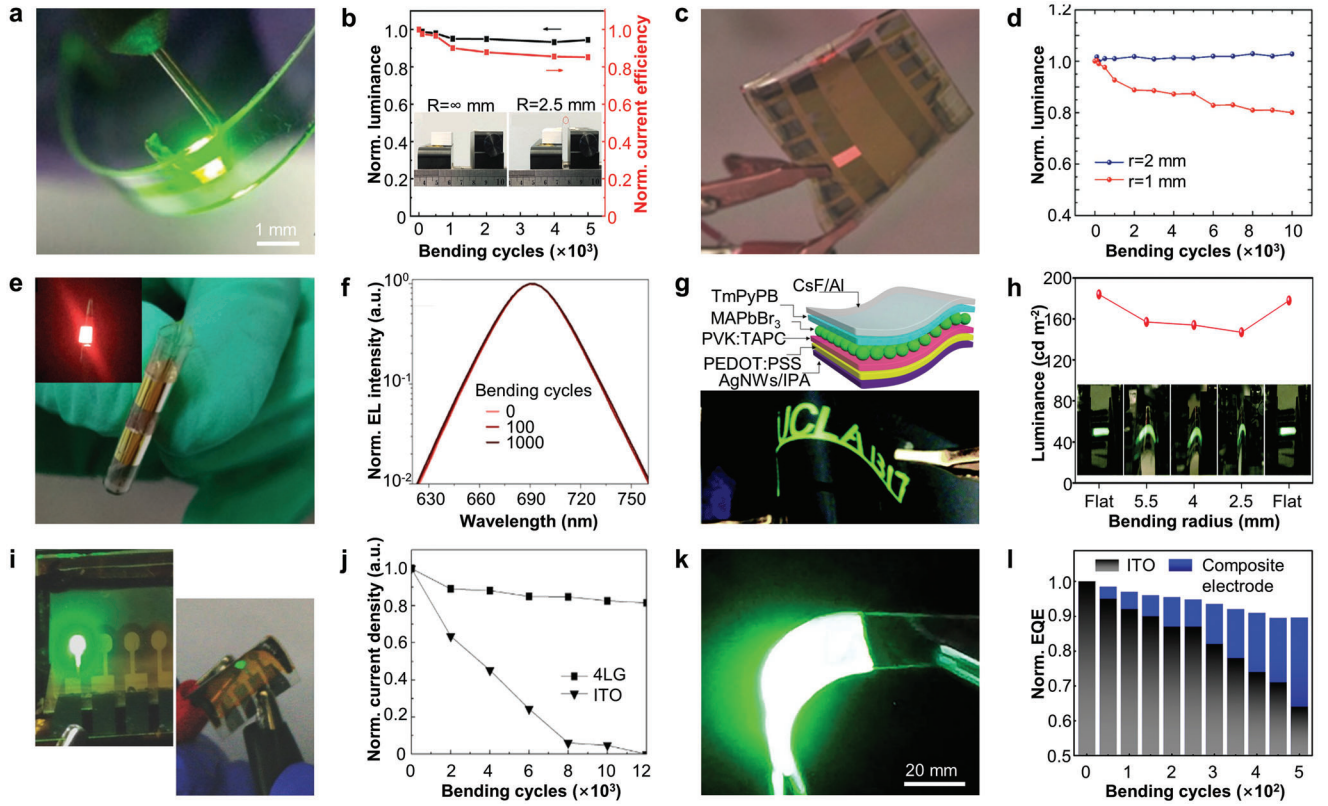

Figure 5. Flexible PeLEDs without encapsulation. a) Photograph of working $MAPbBr_3$ PeLEDs fabricated on a flexible PDMS/PET elastomer substrate bent to a curvature radius of 3.5 mm. b) Normalized luminance and current efficiency measured at various bending cycles with a curvature radius of 2.5 mm. The insets show the experimental setup for the bending test at pristine and bent states. Reproduced with permission.[205] Copyright 2021, Wiley-VCH GmbH. c) Digital photograph of quasi-2D $MAPbI_3$ PeLEDs doped with FPMAI additives on PI/AgNWs substrates. d) Normalized EQE versus bending cycles at bending radii of 1 and 2 mm for flexible red PeLEDs with FPMAI. Reproduced with permission.[184] Copyright 2018, Wiley-VCH GmbH. e) Photographs of the flexible $CsPbI_3$ NCs PeLEDs on a photopolymer (NOA63) flexible substrate. The inset is the photograph of PeLEDs operated at 5 V. f) Normalized EL spectra of PeLEDs with different repeated bending cycles. Reproduced with permission.[190] Copyright 2019, Wiley-VCH GmbH. g) Device structure (top) and optical image (bottom) of the flexible $MAPbBr_3$ NCs PeLED composed of AgNW-polymer composite electrode. h) Luminance of the flexible PeLED at various bending radii. Reproduced with permission.[181] Copyright 2017, the Royal Society of Chemistry. i) Photograph of $MAPbBr_3$ PeLEDs with a p-type four-layer graphene anode on glass (left) and PET substrate (right). j) Normalized current density of flexible graphene-based and ITO-based PeLEDs with different bending cycles at a bending radius of 5 mm. Reproduced with permission.[182] Copyright 2017, Wiley-VCH GmbH. k) Photograph of a flexible green quasi-2D $FEA_2Cs_{n-1}Pb_nBr_{3n+1}$ (n = 1–6) PeLED with a mixed-dimensional MXene-based composite electrode operating at 5 V. l) Normalized EQE of ITO and composite electrode-based PeLEDs in bending tests at a bending radius of 1 cm. Reproduced with permission.[200] Copyright 2022, American Chemical Society.

selected because of their popular use in charge transport and blocking layers. Degradation under an atmospheric environment for 120 h and bending fracture were measured for encapsulation layers with various thicknesses from 20 to 50 nm. In the X-ray diffraction pattern, an additional PbI_2 peak (2θ = ≈12.5°) was detected for the air-exposed nonencapsulated perovskite film owing to phase separation into residual perovskite and PbI_2. However, all the encapsulated samples maintained the original perovskite phase and did not exhibit a PbI_2 peak. The bending fracture was measured by continuously increasing the bending strain up to 2.12% (ϵ_a = ≈2.12%) and visualizing the effect via optical microscopy. For the nonencapsulation layer, linear cracks were initially observed at ϵ_a = ≈1.49%, and the number of cracks increased with increasing bending strain. Conversely, a linear crack was first detected at 1.73% and 1.96% strain in the 50 nm thick PEDOT:PSS and 50 nm thick PS encapsulation layer, respectively. In addition, the nonencapsulated perovskite film exhibited the highest crack density, compared with the encapsulated films for the whole range of bending strain applied (Figure 6b).

Cheng et al. fabricated PET/AgNWs/PEDOT:PSS/Perovskite/TPBi/LiF/Al PeLEDs with epoxy top-encapsulation.[139] AgNWs (diameter = 40 nm, length = 20–30 μm) were spin cast onto flexible PET substrates to form a transparent electrode (transmittance > 80%). The AgNW-based electrode exhibited a sheet resistance of <25 Ω sq^{-1} and root-mean-square (RMS) roughness of 20 nm. To decrease the electrode roughness, a PEDOT:PSS layer (45 nm) was spin-coated onto the patterned AgNWs, resulting in a low RMS roughness of ≈6 nm. Therefore, the roughness of the 45 nm thick perovskite film on PET/AgNWs/PEDOT:PSS was almost identical to that on the glass substrate. With this transparent electrode and epoxy encapsulation, flexible PeLEDs exhibited a maximum EQE of 10.1% and maximum CE of 31.0 cd A^{-1} under ambient condition, comparable to the performance of the rigid PeLED (Figure 6c).

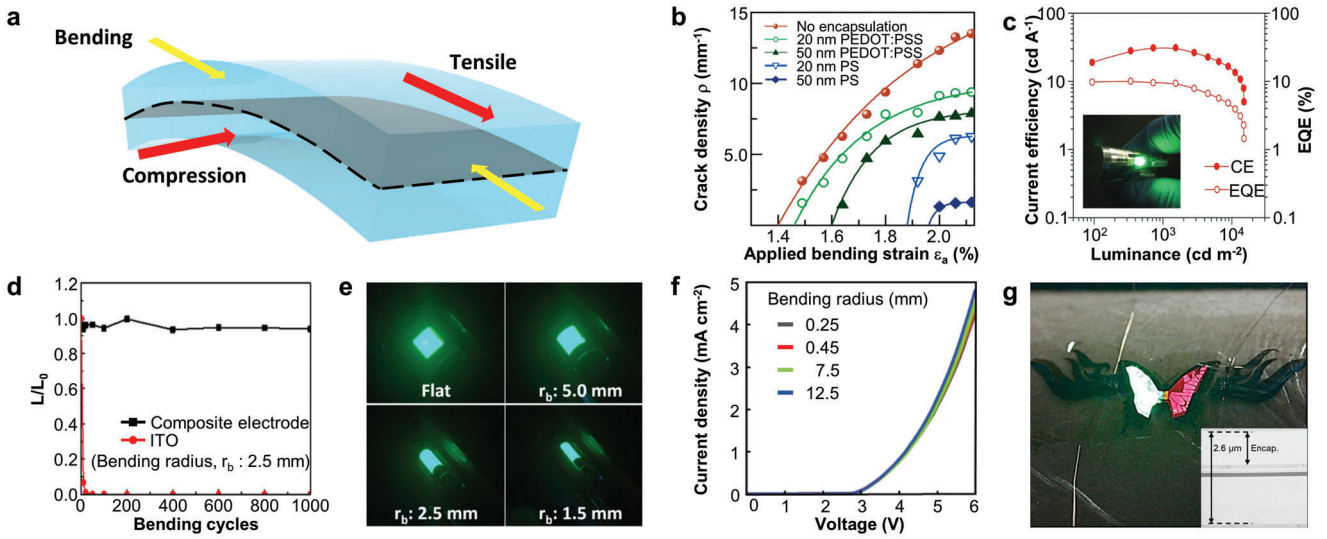

Figure 6. Flexible PeLEDs with encapsulation. a) Schematic of the stress and neutral mechanical plane under mechanical deformation. b) Crack density on nonencapsulated perovskite layer and polymer-encapsulated perovskite layer under applied bending strain. Reproduced with the permission.[221] Copyright 2022, Elsevier. c) CE–*L*–EQE characteristic of PeLEDs with AgNW electrode and epoxy resin top-encapsulation. Reproduced with the permission.[139] Copyright 2018, Wiley-VCH GmbH. d) Cycling test luminance comparison of composite electrode-based PeLEDs and ITO-based PeLEDs at bending radius (r_b) = 2.5 mm. e) Digital photograph of PeLEDs at different bending radii. Reproduced with the permission.[189] Copyright 2019, American Chemical Society. f) *J*–*V* characteristic of PeLEDs at different bending radii. g) Digital photograph of multicolor transfer-printed PeLEDs on human skin; inset displays the FIB image. Reproduced with the permission.[201] Copyright 2022, The American Association for the Advancement of Science.

Lee et al. reported the luminescence performances of PeLEDs with various flexible substrate/electrode combinations (i.e., NOA63/PEDOT:PSS, PET/AgNWs, NOA63/AgNWs, and PEDOT:PSS composite, and PEN/ITO) under bending conditions.[189] The basic structure of the device was flexible substrate/electrode/Zonyl-treated PEDOT:PSS/quasi-2D perovskite/TPBi/LiF/Al. The PeLED was sandwiched between an 80 μm thick flexible substrate (NOA63, PEN, and PET) and 80 μm thick top-encapsulation layer (NOA63) to position the PeLED near the neutral mechanical plane. For NOA63 substrate-based electrode fabrication, PEDOT:PSS (PH 1000) and AgNWs were spin-cast on a glass substrate. Then, NOA63 was spin-cast on the electrode, followed by UV curing. The electrode/substrate was then peeled from the glass substrate. For PEN substrate-based electrode fabrication, AgNWs were spin-cast on the electrode and annealed. The H_2SO_4-treated PEDOT:PSS electrode, AgNW electrode, and composite electrode exhibited 109 Ω sq^{-1} sheet resistance with 85.7% transmittance at 550 nm, 26 Ω sq^{-1} sheet resistance with 93.5% transmittance at 550 nm, and 23.2 Ω sq^{-1} sheet resistance with 90.5% transmittance at 550 nm, respectively. Owing to the composite electrode having the lowest sheet resistance, the flexible PeLEDs showed the highest maximum luminance (L_{max} = 1060 cd m^{-2}), CE (CE_{max} = 17.90 cd A^{-1}), and EQE (EQE_{max} = 3.98%); these were higher than those of the control device (PEN/ITO, EQE_{max} = 2.14%). The composite electrode-based PeLEDs showed no change in sheet resistance per unit initial sheet resistance ($\Delta R/R_0$) for bending radii between 20 and 2.5 mm, maintained 94% of the initial luminance even after 1000 bending cycles (bending radius = 2.5 mm), and maintained 98% of the initial luminance for bending radii between 20 and 2.5 mm; meanwhile, PEN/ITO showed a significant increase in sheet resistance and decrease in luminance (Figure 6d). As shown in Figure 6e, the flexible PeLEDs showed stable light emission until the bending radius of 1.5 mm.

To enable conformal contact on various curvilinear surfaces such as human skin, leaves, glass rods, and the edge of blades, decreasing the thickness of substrate and encapsulation layer is essential.[223,2] Kwon et al. reported 2.6 μm thick ultrathin flexible PeLEDs that included encapsulation layers; parylene/epoxy/ITO/PEDOT:PSS/poly-TPD/perovskite/TPBi/LiF/Al/parylene.[201] PeLEDs with parylene/epoxy double-encapsulation had low turn-on voltages (<3.0 V) and high EQEs (≈6.2 %). Owing to the 1.3 μm thick parylene/epoxy substrate and a 1.0 μm thick parylene top-encapsulation layer, the fragile ITO electrode could be situated at the neutral mechanical plane of the entire device to minimize stress on the active layer during deformation. Therefore, flexible PeLEDs successfully exhibited stable current densities at various bending radii (12.5, 7.5, 0.45, and 0.25 mm) (Figure 6f). Furthermore, by applying transfer printing to flexible PeLEDs, multicolor flexible PeLEDs on human skin displayed stable luminance (Figure 6g) and maintained stable luminance even when undergoing 10% compression and twist.

6. Application of Flexible PeLEDs

Flexible PeLEDs can be used in a wide range of applications as deformable optoelectronic devices.[224,225] When combined with various device components, flexible PeLEDs can act as an input and output source for wearable devices. They can also work alone as stable data visualization media under deformation. By applying additional structure to flexible PeLEDs, wearable sensor-integrated LEDs such as light-emitting touch-sensitive

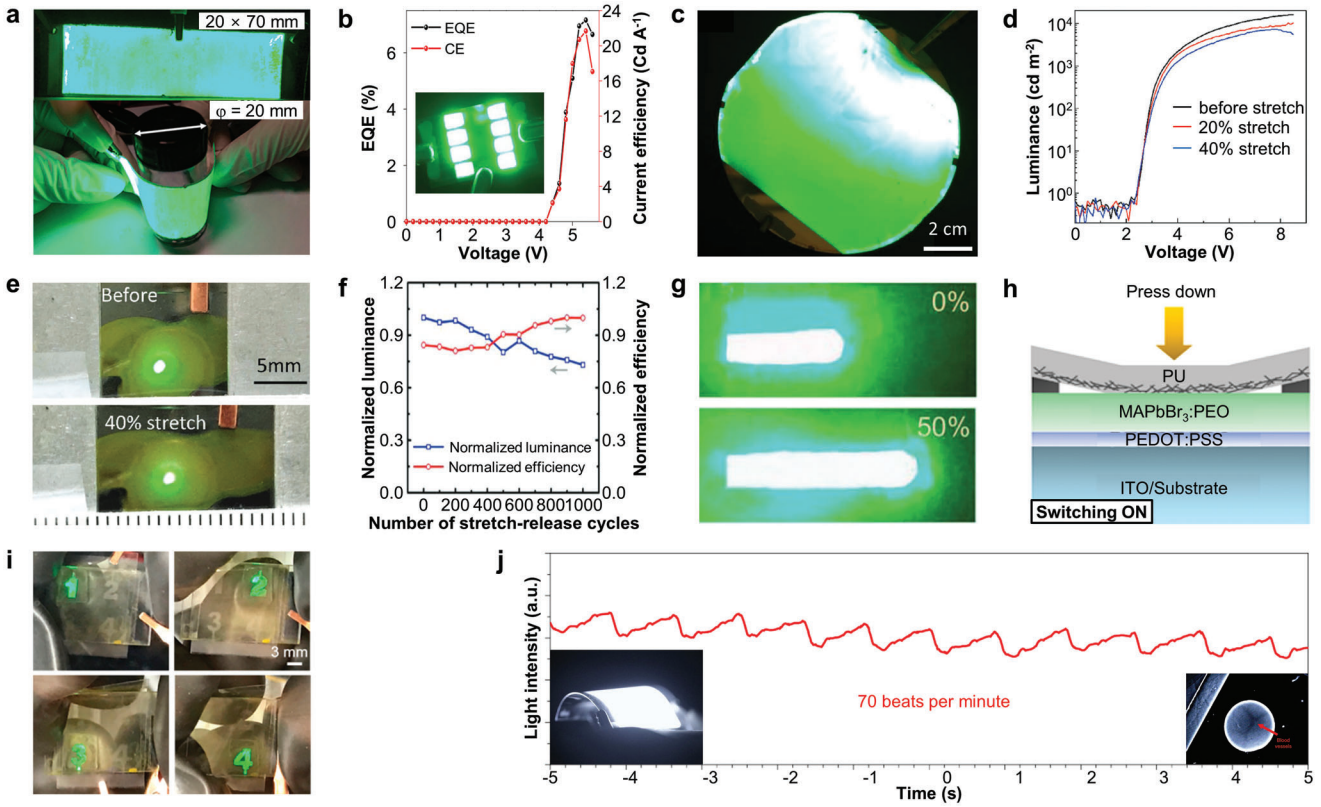

Figure 7. PeLEDs application. a) Photographs of large-scale (70 mm × 20 mm) flexible PeLEDs before (top) and after (bottom) bending at a 20 mm bending radius. Reproduced with the permission.[195] Copyright 2020, American Chemical Society. b) EQE–*V*, CE–*V* characteristic of flexible PeLEDs. c) EL photograph of 4 in. wafer-scale while deformation. Reproduced with the permission.[226] Copyright 2022, Springer Nature. d) *L*–*V* characteristic of stretchable PeLEDs before and after stretching to 20% and 40% strain. e) Photographs of PeLEDs before (top) and after (bottom) stretching with 40% strain at 4 V bias. Reproduced with the permission.[180] Copyright 2017, Wiley-VCH GmbH. f) Normalized luminance and current efficiency versus stretch–release cycles of PeLEDs between 0% and 20% strain. g) Photographs of stretchable PeLEDs before (top) and after (bottom) 50% strain. Reproduced with the permission.[188] Copyright 2019, Wiley-VCH GmbH. h) Schematic illustration of LETD on switching to ON state. i) Photograph of selective illumination (1, 2, 3, 4) with pressure applied on the specific location. Reproduced with the permission.[179] Copyright 2017, American Chemical Society. j) Heart rate monitoring signal with NIR-region PeLEDs; left inset: NIR photographs of the large area (900 mm^2) PeLEDs, right inset: illumination of the subcutaneous blood vessels. Reproduced with the permission.[192] Copyright 2020, Springer Nature.

devices (LETDs) and sensor-embedded photoplethysmography (PPG) sensors can be realized.

To use flexible PeLEDs in future displays (e.g., lighting on various curvilinear surfaces), the development of fabrication technologies for the large-area PeLED is needed. Chen et al. reported large-area flexible PeLEDs (20 mm × 70 mm) using a co-evaporated perovskite film.[195] Thin ITO was introduced as a transparent electrode on a flexible PET substrate. The large-area PeLEDs exhibited a high luminance of 17, 350 cd m^{-2} at 6.5 V, CE_{max} of 10.3 cd A^{-1}, and half-lifetime of more than 400 min at 500 cd m^{-2}. The large-area PeLEDs exhibited successful emission under bending deformations (bending radius of 20 mm) (**Figure 7**a). Zhang et al. reported 4 in. wafer-scale flexible PeLEDs using crystalline perovskite quantum-wire (QW) arrays grown in porous alumina membranes via a close-spaced vapor reaction.[226] The flexible QW arrays were grown on flexible substrate (50 µm thick Al foils and 100 µm thick Corning Willow glass) or on 3D spherical substrates and showed bright and stable luminance while deformation. Hydrophobic QW arrays exhibited 92% of PLQY and 5644 h of half-lifetime in ambient air condition. In addition, the QWs PeLEDs (Al/Al_2O_3/QWs perovskites/CuPC/IZO) exhibited 31 667 cd m^{-2} at 8 V, EQE_{max} of 7.3%, and half-lifetime of 2.9 h at 193 cd m^{-2} (Figure 7b). The 4 in. wafer-scale flexible PeLEDs also showed extremely uniform light emission under deformation (Figure 7c).

The flexible PeLEDs can be also used to develop stretchable type of PeLED. The stretchable devices can be either intrinsically stretchable or structurally stretchable. Intrinsically stretchable PeLEDs can be developed by using inherently stretchable material components.[227] Conducting and semiconducting elastomers can be employed for this approach. However, large-area and high-resolution fabrication as well as achievement of high performance and long-term stability is challenging when it comes to intrinsically stretchable PeLED fabrication. In this review, the application of flexible PeLEDs to the stretchable PeLED by utilizing special structures and device designs will be mainly discussed. Intrinsically stretchable PeLEDs can be fabricated by replacing the fragile ITO with a polymer-based transparent electrode and blending the perovskite layer with polymer. Bade et al. reported intrinsically stretchable PeLEDs

using PEDOT:PSS/PEO as a transparent and stretchable composite electrode, $MAPbBr_3$/PEO composite as the emission layer, and liquid metal (EGaIn) as the top electrode.[180] With fabricate stretchable PeLEDs with aforementioned materials, until the uniaxial stress reached 40%, PeLEDs showed successful emission with 10 148 cd m^{-2} under 20% stretching and 7340 cd m^{-2} under 40% stretching (Figure 7d,e). During the cycling test, the device exhibited stable emission without failure up to 40% strain for 100 cycles.

Li et al. reported structurally stretchable PeLEDs with buckled structures. First, flexible PeLEDs were fabricated with ultrathin (2 μm), transparent (90% transmittance), and low-sheet-resistance (20 Ω sq^{-1}) PI/AgNW electrodes.[188] During the fabrication of the PeLEDs, the PI/AgNW electrode was adhered to the PDMS-coated glass for device flattening. To apply the buckling structure, the flexible PeLEDs fabricated on PDMS-coated glass were transferred to a prestretched very high bonding (VHB) tape. After the transfer-printing, buckling structures were constructed by releasing the strain on the VHB tape, following which PeLEDs can be stretched while applying strain on the VHB tape. As a result, the device exhibited luminescence of 3187 cd m^{-2} under 50% strain, and the device showed analogous EL performance even after 1000 stretch–release cycles under 20% tensile strain (Figure 7f). Even when stretched, PeLEDs maintain initial luminescence efficiencies with stable light emission (9.08 cd A^{-1} at 0% strain, 8.87 cd A^{-1} at 25% strain, and 8.91 cd A^{-1} at 50% strain) (Figure 7g).

LETDs can be applied as wearable sensors for motion detection. In LETDs, the spacer between the emissive layer and the electrode blocks charge transfer within the device when external pressure is not applied; when an external pressure is applied to the electrode, the electrode and emissive layer come in direct contact with each other, allowing charge carriers to successfully move, operating the LETD. Chou et al. reported a flexible perovskite LETD (PeLETD) with a PET/ITO/PEDOT:PSS/$MAPbBr_3$:PEO/spacer/AgNW–PU composite (Figure 7h).[179] To create a gap between the emissive layer and the electrode, 100 μm thick double-sided tape was used as spacer. Using a flexible AgNW–PU composite, the device could be successfully bent up to 6 mm bending radius. The AgNW–PU composite-based flexible electrode showed stable sheet resistance for 100 mechanical deformation cycles with 16% strain as well as repeated adhesion and peeling tests. Under pressure applied onto the AgNW–PU electrode, the device exhibited 1030 cd m^{-2} EL. Further, arrayed PeLTEDs were fabricated using AgNWs patterned via spray coating. When pressure was applied to a specific location, only the touched area was illuminated (Figure 7i).

PeLEDs can be used as a light source for PPG sensors in wearable biomedical sensing applications. The wearable PPG sensor can monitor the heart rate noninvasively by measuring changes in the blood volume flowing through the blood vessels from the measurement of changes in the light absorption. However, nonconformal contact between the rigid sensor and the skin results in an inaccurate signal. To solve this problem, flexible PPG sensors have been extensively investigated.[228] Zhao and Tan reported a large-area PPG sensor with NIR (799 nm) PeLEDs made of a $FAPbI_3$ emission layer.[192] With the PET substrate, the device exhibited stable illumination during bending. By combining PeLEDs with a silicon photodiode to detect scattered light, fluctuation in the photocurrent can be measured. In addition, using large-area (900 mm^2) NIR-PeLEDs, muscle performance can be monitored, and blood vessel blockage and blood clot can be detected (Figure 7j).

7. Conclusion

In this review, we summarize recent advances for flexible PeLEDs, including light-emitting material engineering, device structure engineering, and encapsulation layer modifications for applying flexibility, and multifaceted applications of flexible PeLEDs. PeLEDs have shown remarkable progresses in optical characteristics, including vivid luminance with high color purity (FWHM <20 nm) and EQEs over 20% in green, red, and NIR region. However, PeLEDs still have challenges including low efficiency of blue PeLEDs, low operational stability, and pixelization for the full color displays.

Especially, the stability of perovskite materials in ambient condition is the key issue. Adding mixed anionic and/or cationic dopants and synthesizing core–shell structure for surface passivation of perovskites via post-treatment are frequently utilized to improve stability of perovskites against oxygen, water, and heat exposure. A recent approach using in situ formation of PeNCs[92] suggests an effective way of producing highly stable PeLEDs. In addition, to ensure the feasibility of flexible PeLEDs in daily life, it is imperative to devise ultrathin encapsulation layers capable of safeguarding against exposure to oxygen/moisture. Among the promising strategies, ultrathin organic/inorganic alternating encapsulation[229] is expected to be effective in conferring high durability to flexible PeLEDs.

Another significant hurdle in flexible PeLEDs is the lower optical efficiency compared to their rigid counterparts. This challenge is primarily attributed to the high resistance of flexible transparent anodes, which impairs the charge injection into emitting layer of flexible PeLEDs. To address this issue, several materials, such as Ag NWs, 2D materials, and conductive polymers, have been proposed as viable alternatives to rigid inorganic transparent electrode (e.g., ITO, AZO), but their sheet resistance is still much higher than inorganic transparent electrodes. Thus, the development of noble transparent anode with high conductivity and transparency is imperative for enhancing the efficiency of flexible PeLEDs.

Furthermore, one of the biggest challenges to achieve commercial full color flexible perovskite displays is development of high-definition perovskite patterning techniques including photolithography, inkjet printing, and transfer printing.[230-232] Red/green/blue pixelization of perovskite is a key parameter to achieve ultrahigh-resolution displays for AR/VR applications. In order to minimize the power consumption of the displays, it is necessary to satisfy high definition and high luminance efficiency of PeLEDs simultaneously.

Acknowledgements

J.H.J. and S.L. contributed equally to this work. This research was supported by IBS-R006-D1 and IBS-R006-A1. This work was supported by the National Research Foundation of Korea (NRF) grant funded by the Korean government (MSIT) (grant nos. 2021R1C1C1007997, 2021R1C1C1007844, and 2022R1A5A6000846). This study was supported by Samsung Research Funding & Incubation Center of Samsung Electronics under Project

Number SRFC-MA2002-03. This work was supported by 2023 research fund (1.230013.01) of UNIST. This work was supported by the DGIST R&D Program of the Ministry of Science and ICT (22-SENS2-6).

Conflict of Interest

The authors declare no conflict of interest.

Keywords

deformable displays, flexible displays, perovskites, perovskite light-emitting diodes

Received: November 28, 2022
Revised: March 28, 2023
Published online: June 8, 2023

[1] C. W. Tang, S. A. VanSlyke, *Appl. Phys. Lett.* **1987**, *51*, 913.
[2] U. Mitschke, P Bauerle, *J. Mater. Chem.* **2000**, *10*, 1471.
[3] M. A. Baldo, D. F. O'brien, Y. You, A. Shoustikov, S. Sibley, M. E. Thompson, S. R. Forrest, *Nature* **1998**, *395*, 151.
[4] B. S. Mashford, M. Stevenson, Z. Popovic, C. Hamiltion, Z. Zhou, C. Breen, J. Steckel, V. Bulovic, M. Bawendi, S. Coe-Sullivan, P. T. Kazlas, *Nat. Photonics* **2013**, *7*, 407.
[5] J. Kwak, W. K. Bae, D. Lee, I. Park, J. Lim, M. Park, H. Cho, H. Woo, D. Y. Yoon, K. Char, S. Lee, C. Lee, *Nano Lett.* **2012**, *12*, 2362.
[6] J. Yang, M. K. Choi, D.-H. Kim, T. Hyeon, *Adv. Mater.* **2016**, *28*, 1176.
[7] J. Yang, M. K. Choi, U J. Yang, S. Y. Kim, Y. S. Kim, J. H. Kim, D.-H. Kim, T. Hyeon, *Nano Lett.* **2021**, *21*, 26.
[8] M. K. Choi, J. Yang, D. C. Kim, Z. Dai, J. Kim, H. Seung, V. S. Kale, S. J. Sung, C. R. Park, N. Lu, T. Hyeon, D.-H. Kim, *Adv. Mater.* **2018**, *30*, 1703279.
[9] Z.-K. Tan, R. S. Moghaddam, M. L. Lai, P. Docampo, R. Higler, F. Deschler, M. Price, A. Sadhanala, L. M. Pazos, D. Credgington, F. Hanusch, T. Bein, H. J. Snaith, R. H. Friend, *Nat. Nanotechnol.* **2014**, *9*, 687.
[10] X. Zhang, H. Lin, H. Huang, C. Reckmeier, Y. Zhang, W. C. H. Choy, A. L. Rogach, *Nano Lett.* **2016**, *16*, 1415.
[11] K. Lin, J. Xing, L. N. Quan, F. P. G. d. Arquer, X. Gong, J. Lu, L. Xie, W. Zhao, D. Zhang, C. Yan, W. Li, X. Liu, Y. Lu, J. Kirman, E. H. Sargent, Q. Xiong, Z. Wei, *Nature* **2018**, *562*, 245.
[12] Y. Cao, N. Wang, H. Tian, J. Guo, Y. Wei, H. Chen, Y. Miao, W. Zou, K. Pan, Y. He, H. Cao, Y. Ke, M. Xu, Y. Wang, M. Yang, K. Du, Z. Fu, D. Kong, D. Dai, Y. Jin, G. Li, H. Li, Q. Peng, J. Wang, W. Huang, *Nature* **2018**, *562*, 249.
[13] F. Liu, Y. Zhang, C. Ding, S. Kobayashi, T. Izuishi, N. Nakazawa, T. toyoda, T. Ohta, S. Hayase, T. Minemoto, K. Yoshino, S. Dai, Q. Shen, *ACS Nano* **2017**, *11*, 10373.
[14] S. D. wolf, J. Holovsky, S.-J. Moon, P. Loper, B. Niesen, M. Ledinsky, F.-J. Haug, J.-H. Yum, C. Ballif, *J. Phys. Chem. Lett.* **2014**, *5*, 1035.
[15] J. Maes, L. Balcaen, E. Drijvers, Q. Zhao, J. D. Roo, A. Vantomme, F. Vanhaecke, P. Geiregat, Z. Hens, *J. Phys. Chem. Lett.* **2018**, *9*, 3093.
[16] A. Swarnkar, R. Chulliyil, V. K. Ravi, M. Irfanullah, A. Chowdhury, A. Nag, *Angew. Chem., Int. Ed.* **2015**, *54*, 15424.
[17] L. C. Schmidt, A. Pertegas, S. G. -Carrero, O. Malinkiewicz, S. Agouram, G. M. Espallargas, H. J. Bolink, R. E. Galian, J. P. Prieto, *J. Am. Chem. Soc.* **2014**, *136*, 850.
[18] W.-J. Yin, J.-H. Yang, J. Kang, Y. Yan, S.-H. Wei, *J. Mater. Chem. A* **2015**, *3*, 8926.
[19] G. Gustafsson, Y. Cao, G. M. Treacy, F. Klavetter, N. Colaneri, A. J. Heeger, *Nature* **1992**, *357*, 477.
[20] T.-H. Han, Y. Lee, M.-R. Choi, S.-H. Woo, S.-H. Bae, B. H. Hong, J.-H. Ahn, T.-W. Lee, *Nat. Photonics* **2012**, *6*, 105.
[21] M. K. Choi, J. Yang, K. Kang, D. C. Kim, C. Choi, C. Park, S. J. Kim, S. I. Chae, T.-H. Kim, J. H. Kim, T. Hyeon, D.-H. Kim, *Nat. Commun.* **2015**, *6*, 7149.
[22] Y.-H. Kim, H. Cho, J. H. Heo, T.-S. Kim, N. Myoung, C.-L. Lee, S. H. Im, T.-W. Lee, *Adv. Mater.* **2015**, *27*, 1248.
[23] D. Lanman, D. Luebke, *ACM Trans. Graphics* **2013**, *32*, 220.
[24] M. K. Choi, J. Yang, T. Hyeon, D.-H. Kim, *npj Flexible Electron.* **2018**, *2*, 10.
[25] M. Kaltenbrunner, T. sekitani, J. Reeder, T. Yokota, K. Kuribara, T. Tokuhara, M. Drack, R. Schwodiauer, I. Graz, S. Bauer-Gogonea, S. Bauer, T. Someya, *Nature* **2013**, *499*, 458.
[26] S. Jo, S. Cho, U. J. Yang, G.-S. Hwang, S. Baek, S.-H. Kim, S. H. Heo, J.-Y. Kim, M. K. Choi, J. S. Son, *Adv. Mater.* **2021**, *33*, 2100066.
[27] J. H. Koo, D. C. Kim, H. J. Shim, T.-H. Kim, D.-H. Kim, *Adv. Funct. Mater.* **2018**, *28*, 1801834.
[28] H. Seung, C. Choi, D. C. Kim, J. S. Kim, J. H. Kim, J. Kim, S. I. Park, J. A. Lim, J. Yang, M. K. Choi, T. Hyeon, D.-H. Kim, *Sci. Adv.* **2022**, *8*, eabq3101.
[29] S. Liu, Y. Rao, H. Jang, P. Tan, N. Lu, *Matter* **2022**, *5*, 1104.
[30] M. S. Kim, G. J. Lee, C. Choi, M. S. Kim, M. Lee, S. Liu, K. W. Cho, H. M. Kim, H. Cho, M. K. Choi, N. Lu, Y. M. Song, D.-H. Kim, *Nat. Electron.* **2020**, *3*, 546.
[31] M. Lee, G. J. Lee, H. J. Jang, E. Joh, H. Cho, M. S. Kim, H. M. Kim, K. M. Kang, J. H. Lee, M. Kim, H. Jang, J.-E. Yeo, F. Durand, N. Lu, D.-H. Kim, Y. M. Song, *Nat. Electron.* **2022**, *5*, 452.
[32] S.-Y. Kim, J. H. Bong, C. Kim, W. S. Hwang, T.-S. Kim, B. J. Cho, *Adv. Mater. Interfaces* **2017**, *4*, 1700618.
[33] J. A. Vigil, A. Hazarika, J. M. Luther, M. F. Toney, *ACS Energy Lett.* **2020**, *5*, 2475.
[34] G. E. Eperon, D. S. Ginger, *ACS Energy Lett.* **2017**, *2*, 1190.
[35] T. Chiba, Y. Hayashi, H. Ebe, K. Hoshi, J. Sato, S. Sato, Y.-J. Pu, S. Ohisa, J. Kido, *Nat. Photonics* **2018**, *12*, 681.
[36] C. Sun, Y. Jiang, M. Cui, L. Qiao, J. Wei, Y. Huang, L. Zhang, T. He, S. Li, H.-Y. Hsu, C. Qin, R. Long, M. Yuan, *Nat. Commun.* **2021**, *12*, 2207.
[37] K. Tanaka, R. Ozawa, T. Umebayashi, K. Asai, K. Ema, T. Kondo, *Phys. E* **2005**, *25*, 378.
[38] D. Zhu, M. L. Zaffalon, J. Zito, F. Cova, F. Meinardi, L. De Trizio, I. Infante, S. Brovelli, L. Manna, *ACS Energy Lett.* **2021**, *6*, 2283.
[39] C. J. Howard, H. T. Stokes, *Acta Crystallogr., Sect. A: Found. Adv.* **2005**, *61*, 93.
[40] A. Mannodi-Kanakkithodi, M. K. Y. Chan, *Energy Environ. Sci.* **2022**, *15*, 1930.
[41] J. Kim, D. Seong, H. Kwon, S. Jin, H. Kim, Y. Kim, Y. Jeong, K. Lee, S. J. Kwon, M. Shin, D. Son, I. S. Kim, *ACS Nano* **2021**, *15*, 20127.
[42] W. Lee, Y. J. Yoo, J. Park, J. H. Ko, Y. J. Kim, H. Yun, D. H. Kim, Y. M. Song, D.-H. Kim, *Nat. Commun.* **2022**, *13*, 1946.
[43] D. Meggiolaro, S. G. Motti, E. Mosconi, A. J. Barker, J. Ball, C. A. R. Perini, F. Deschler, A. Petrozza, F. D. Angelis, *Energy Environ. Sci.* **2018**, *11*, 702.
[44] B. Saparov, D. B. Mitzi, *Chem. Rev.* **2016**, *116*, 4558.
[45] Z. Li, M. Yang, J.-S. Park, S.-H. Wei, J. J. Berry, K. Zhu, *Chem. Mater.* **2016**, *28*, 284.
[46] V. M. Goldschmidt, *Naturwissenschaften* **1926**, *14*, 477.
[47] L. N. Quan, B. P. Rand, R. H. Friend, S. G. Mhaisalkar, T.-W. Lee, E. H. Sargent, *Chem. Rev.* **2019**, *119*, 7444.
[48] J. S. Manser, J. A. Christians, P. V. Kamat, *Chem. Rev.* **2016**, *116*, 12956.
[49] A. Amat, E. Mosconi, E. Ronca, C. Quarti, P. Umari, M. K. Nazeeruddin, M. Grätzel, F. D. Angelis, *Nano Lett.* **2014**, *14*, 3608.

[50] G. J. Man, C. Kamal, A. Kalinko, D. Phuyal, J. Acharya, S. Mukherjee, P. K. Nayak, H. Rensmo, M. Odelius, S. M. Butorin, *Nat. Commun.* **2022**, *13*, 3839.
[51] H. Cho, Y.-H. Kim, C. Wolf, H.-D. Lee, T.-W. Lee, *Adv. Mater.* **2018**, *30*, 1704587.
[52] M. R. Linaburg, E. T. McClure, J. D. Majher, P. M. Woodward, *Chem. Mater.* **2017**, *29*, 3507.
[53] E. Mosconi, P. Umari, F. D. Angelis, *J. Mater. Chem. A* **2015**, *3*, 9208.
[54] A. Swarnkar, W. J. Mir, A. Nag, *ACS Energy Lett.* **2018**, *3*, 286.
[55] W. v. d. Stam, J. J. Geuchies, T. Altantzis, K. H. W. v. d. Bos, J. D. Meeldijk, S. V. Aert, S. Bals, D. Vanmaekelbergh, C. d. M. Donega, *J. Am. Chem. Soc.* **2017**, *139*, 4087.
[56] C.-H. Li, M.-Y. Liao, C.-H. Chena, C.-C. Chueh, *J. Mater. Chem. C* **2020**, *8*, 4294.
[57] L. Protesescu, S. Yakunin, M. I. Bodnarchuk, F. Krieg, R. Caputo, C. H. Hendon, R. X. Yang, A. Walsh, M. V. Kovalenko, *Nano Lett.* **2015**, *15*, 3692.
[58] Q. A. Akkerman, V. D'Innocenzo, S. Accornero, A. Scarpellini, A. Petrozza, M. Prato, L. Manna, *J. Am. Chem. Soc.* **2015**, *137*, 10276.
[59] K. Zheng, Q. Zhu, M. Abdellah, M. E. Messin, W. Zhang, A. Generalov, Y. Niu, L. Ribaud, S. E. Canton, T. Pullerits, *J. Phys. Chem. Lett.* **2015**, *6*, 2969.
[60] A. Fakharuddin, M. K. Gangishetty, M. Abdi-Jalebi, S.-H. Chin, Abd. R. b. Mohd Yusoff, D. N. Congreve, W. Tress, F. Deschler, M. Vasilopoulou, H. J. Bolink, *Nat. Electron.* **2022**, *5*, 203.
[61] M. C. Weidman, A. J. Goodman, W. A. Tisdale, *Chem. Mater.* **2017**, *29*, 5019.
[62] E. Mosconi, P. Umari, F. D. Angelis, *Adv. Mater.* **2016**, *28*, 7515.
[63] T. Bai, X. Wang, Z. Wang, S. Ji, X. Meng, Q. Wang, R. Zhang, P. Han, K.-L. Han, J. Chen, F. Liu, B. Yang, *Angew. Chem., Int. Ed.* **2023**, *62*, e202213240.
[64] P. Tyagi, S. M. Arveson, W. A. Tisdale, *J. Phys. Chem. Lett.* **2015**, *6*, 1911.
[65] D. B. Mitzi, S. Wang, C. A. Field, C. A. Chess, A. M. Guloy, *Science* **1995**, *267*, 1473.
[66] O. Nazarenko, M. R. Kotyrba, S. Yakunin, M. Aebli, G. Rainò, B. M. Benin, M. Wörle, M. V. Kovalenko, *J. Am. Chem. Soc.* **2018**, *140*, 3850.
[67] X. Li, P. Guo, M. Kepenekian, I. Hadar, C. Katan, J. Even, C. C. Stoumpos, R. D. Schaller, M. G. Kanatzidis, *Chem. Mater.* **2019**, *31*, 3582.
[68] M. D. Smith, H. I. Karunadasa, *Acc. Chem. Res.* **2018**, *51*, 619.
[69] T. Hu, M. D. Smith, E. R. Dohner, M. J. Sher, X. Wu, M. T. Trinh, A. Fisher, J. Corbett, X. Y. Zhu, H. I. Karunadasa, A. M. Lindenberg, *J. Phys. Chem. Lett.* **2016**, *7*, 2258.
[70] M. Ren, S. Cao, J. Zhao, B. Zou, R. Zeng, *Nano-Micro Lett.* **2021**, *13*, 163.
[71] S. N. Ruddlesden, P. Popper, *Acta Crystallogr.* **1957**, *10*, 538.
[72] S. N. Ruddlesden, P. Popper, *Acta Crystallogr.* **1958**, *11*, 54.
[73] M. Dion, M. Ganne, M. Tournoux, *Mater. Res. Bull.* **1981**, *16*, 1429.
[74] A. J. Jacobson, J. W. Johnson, J. T. Lewandowski, *Inorg. Chem.* **1985**, *24*, 3727.
[75] T. L. Leung, I. Ahmad, A. A. Syed, A. M. C. Ng, J. Popović, A. B. Djurišić, *Commun. Mater.* **2022**, *3*, 63.
[76] I. C. Smith, E. T. Hoke, D. Solis-Ibarra, M. D. McGehee, H. I. Karunadasa, *Angew. Chem., Int. Ed.* **2014**, *53*, 11232.
[77] L. Mao, W. Ke, L. Pedesseau, Y. Wu, C. Katan, J. Even, M. R. Wasielewski, C. C. Stoumpos, M. G. Kanatzidis, *J. Am. Chem. Soc.* **2018**, *140*, 3775.
[78] C. M. M. Soe, C. C. Stoumpos, M. Kepenekian, B. Traoré, H. Tsai, W. Nie, B. Wang, C. Katan, R. Seshadri, A. D. Mohite, J. Even, T. J. Marks, M. G. Kanatzidis, *J. Am. Chem. Soc.* **2017**, *139*, 16297.
[79] O. Nazarenko, M. R. Kotyrba, M. Worle, E. Cuervo-Reyes, S. Yakunin, M. V. Kovalenko, *Inorg. Chem.* **2017**, *56*, 11552.
[80] D. H. Cao, C. C. Stoumpos, O. K. Farha, J. T. Hupp, M. G. Kanatzidis, *J. Am. Chem. Soc.* **2015**, *137*, 7843.
[81] I. H. Park, L. Chu, K. Leng, Y. F. Choy, W. Liu, I. Abdelwahab, Z. Zhu, Z. Ma, W. Chen, Q. H. Xu, *Adv. Funct. Mater.* **2019**, *29*, 1904810.
[82] Y. Lei, G. Peng, H. Wang, G. Wang, S. Yang, Q. Wang, Z. Li, Z. Jin, *Adv. Mater. Interfaces* **2022**, *9*, 2201501.
[83] S. Ahmad, P. Fu, S. Yu, Q. Yang, X. Liu, X. Wang, X. Wang, X. Guo, C. Li, *Joule* **2019**, *3*, 794.
[84] Y. Zhang, P. Wang, M.-C. Tang, D. Barrit, W. Ke, J. Liu, T. Luo, Y. Liu, T. Niu, D.-M. Smilgies, Z. Yang, Z. Liu, S. Jin, M. G. Kanatzidis, A. Amassian, S. F. Liu, K. Zhao, *J. Am. Chem. Soc.* **2019**, *141*, 2684.
[85] L. Zhang, C. Sun, T. He, Y. Jiang, J. Wei, Y. Huang, M. Yuan, *Light: Sci. Appl.* **2021**, *10*, 61.
[86] Z. Li, M. Yang, J.-S. Park, S.-H. Wei, J. J. Berry, K. Zhu, *Nat. Photonics* **2016**, *10*, 406.
[87] V. D'Innocenzo, G. Grancini, M. J. P. Alcocer, A. R. S. Kandada, S. D. Stranks, M. M. Lee, G. Lanzani, H. J. Snaith, A. Petrozza, *Nat. Commun.* **2014**, *5*, 3586.
[88] S. Sun, M. Lu, X. Gao, Z. Shi, X. Bai, W. W. Yu, Y. Zhang, *Adv. Sci.* **2021**, *8*, 2102689.
[89] L. N. Quan, M. Yuan, R. Comin, O. Voznyy, E. M. Beauregard, S. Hoogland, A. Buin, A. R. Kirmani, K. Zhao, A. Amassian, D. H. Kim, E. H. Sargent, *J. Am. Chem. Soc.* **2016**, *138*, 2649.
[90] Y. Jin, Z.-K. Wang, S. Yuan, Q. Wang, C. Qin, K.-L. Wang, C. Dong, M. Li, Y. Liu, L.-S. Liao, *Adv. Funct. Mater.* **2020**, *30*, 1908339.
[91] Z. Yuan, C. Zhou, Y. Tian, Y. Shu, J. Messier, J. C. Wang, L. J.van de Burgt, K. Kountouriotis, Y. Xin, E. Holt, K. Schanze, R. Clark, T. Siegrist, B. Ma, *Nat. Commun.* **2017**, *8*, 14051.
[92] H. Tanino, W. W. Ruhle, K. Takahashi, *Phys. Rev. B* **1988**, *38*, 12716.
[93] S. Tomimoto, S. Saito, T. Suemoto, J. Takeda, S. Kurita, *Phys. Rev. B* **2002**, *66*, 155112.
[94] A. Trigui, H. Abid, A. Mlayah, Y. Abid, *Synth. Met.* **2012**, *162*, 1731.
[95] X. Wu, M. T. Trinh, D. Niesner, H. Zhu, Z. Norman, J. S. Owen, O. Yaffe, B. J. Kudisch, X.-Y. Zhu, *J. Am. Chem. Soc.* **2015**, *137*, 2089.
[96] M. I. Saidaminov, J. Almutlaq, S. Sarmah, I. Dursun, A. A. Zhumekenov, R. Begum, J. Pan, N. Cho, O. F. Mohammed, O. M. Bakr, *ACS Energy Lett.* **2016**, *1*, 840.
[97] A. Dey, J. Ye, A. De, E. Debroye, S. K. Ha, E. Bladt, A. S. Kshirsagar, Z. Wang, J. Yin, Y. Wang, L. N. Quan, F. Yan, M. Gao, X. Li, J. Shamsi, T. Debnath, M. Cao, M. A. Scheel, S. Kumar, J. A. Steele, M. Gerhard, L. Chouhan, K. Xu, X.-G. Wu, Y. Li, Y. Zhang, A. Dutta, C. Han, I. Vincon, A. L. Rogach, et al., *ACS Nano* **2021**, *15*, 10775.
[98] H. Lin, C. Zhou, Y. Tian, T. Siegrist, B. Ma, *ACS Energy Lett.* **2018**, *3*, 54.
[99] S. Yuan, Z.-K. Wang, M.-P. Zhuo, Q.-S. Tian, Y. Jin, L.-S. Liao, *ACS Nano* **2018**, *12*, 9541.
[100] V. K. Ravi, S. Saikia, S. Yadav, V. V. Nawale, A. Nag, *ACS Energy Lett.* **2020**, *5*, 1794.
[101] Y.-H. Kim, C. Wolf, Y.-T. Kim, H. Cho, W. Kwon, S. Do, A. Sadhanala, C. G. Park, S.-W. Rhee, S. H. Im, R. H. Friend, T.-W. Lee, *ACS Nano* **2017**, *11*, 6586.
[102] G. Nedelcu, L. Protesescu, S. Yakunin, M. I. Bodnarchuk, M. J. Grotevent, M. V. Kovalenko, *Nano Lett.* **2015**, *15*, 5635.
[103] R. E. Brandt, V. Stevanovic, D. S. Ginley, T. Buonassisi, *MRS Commun.* **2015**, *5*, 265.
[104] M. V. Kovalenko, L. Protesescu, M. I. Bodnarchuk, *Science* **2017**, *358*, 745.
[105] R. E. Brandt, J. R. Poindexter, P. Gorai, R. C. Kurchin, R. L. Z. Hoye, L. Nienhaus, M. W. B. Wilson, J. A. Polizzotti, R. Sereika, R. Žaltauskas, L. C. Lee, J. L. MacManus-Driscoll, M. Bawendi, V. Stevanović, T. Buonassisi, *Chem. Mater.* **2017**, *29*, 4667.
[106] H. J. An, S. D. Baek, D. H. Kim, J.-M. Myoung, *Adv. Funct. Mater.* **2022**, *32*, 2112849.

[107] Y. Shen, L.-P. Cheng, Y.-Q. Li, W. Li, J.-D. Chen, S.-T. Lee, J.-X. Tang, *Adv. Mater.* **2019**, *31*, 1901517.
[108] P. Vashishtha, M. Ng, S. B. Shivarudraiah, J. E. Halpert, *Chem. Mater.* **2019**, *31*, 83.
[109] I.-B. Kim, Y.-J. Kim, D.-Y. Kim, S.-Y. Jang, *Macromol. Res.* **2022**, *30*, 391.
[110] V. M. Arivunithi, H.-Y. Park, S. S. Reddy, Y. Do, H. Park, E.-S. Shin, Y.-Y. Noh, M. Song, S.-H. Jin, *Macromol. Res.* **2021**, *29*, 149.
[111] H. Cho, S.-H. Jeong, M.-H. Park, Y.-H. Kim, C. Wolf, C.-L. Lee, J. H. Heo, A. Sadhanala, N. Myoung, S. Yoo, S. H. Im, R. H. Friend, T. W. Lee, *Science* **2015**, *350*, 1222.
[112] R. Khan, S. Chu, Z. Li, K. O. Ighodalo, W. Chen, Z. Xiao, *Adv. Funct. Mater.* **2022**, *32*, 2203650.
[113] Y. Ling, Y. Tian, X. Wang, J. C. Wang, J. M. Knox, F. Perez-Orive, Y. Du, L. Tan, K. Hanson, B. Ma, H. Gao, *Adv. Mater.* **2016**, *28*, 8983.
[114] J. Niu, D. Yang, X. Ren, Z. Yang, Y. Liu, X. Zhu, W. Zhao, S. Liul, *Org. Electron.* **2017**, *48*, 165.
[115] K. Sim, T. Nakao, M. Sasase, S. Iimura, J. Kim, H. Hosono, *Small* **2022**, *18*, 2202298.
[116] Y.-H. Kim, S. Kim, A. Kakekhani, J. Park, J. Park, Y.-H. Lee, H. Xu, S. Nagane, R. B. Wexler, D.-H. Kim, S. H. Jo, L. Martínez-Sarti, P. Tan, A. Sadhanala, G.-S. Park, Y.-W. Kim, B. Hu, H. J. Bolink, S. Yoo, R. H. Friend, A. M. Rappe, T.-W. Lee, *Nat. Photonics* **2021**, *15*, 148.
[117] M. Yuan, L. N. Quan, R. Comin, G. Walters, R. Sabatini, O. Voznyy, S. Hoogland, Y. Zhao, E. M. Beauregard, P. Kanjanaboos, Z. Lu, D. H. Kim, E. H. Sargent, *Nat. Nanotechnol.* **2016**, *11*, 872.
[118] L. N. Quan, Y. Zhao, F. P. G. d. Arquer, R. Sabatini, G. Walters, O. Voznyy, R. Comin, Y. Li, J. Z. Fan, H. Tan, J. Pan, M. Yuan, O. M. Bakr, Z. Lu, D. H. Kim, E. H. Sargent, *Nano Lett.* **2017**, *17*, 3701.
[119] J. S. Kim, J.-M. Heo, G.-S. Park, S.-J. Woo, C. Cho, H. J. Yun, D.-H. Kim, J. Park, S.-C. Lee, S.-H. Park, E. Yoon, N. C. Greenhan, T.-W. Lee, *Nature* **2022**, *611*, 688.
[120] W. Deng, X. Xu, X. Zhang, Y. Zhang, X. Jin, L. Wang, S.-T. Lee, J. Jie, *Adv. Funct. Mater.* **2016**, *26*, 4797.
[121] L. Wang, Z. Shi, Z. Ma, D. Yang, F. Zhang, X. Ji, M. Wang, X. Chen, G. Na, S. Chen, D. Wu, Y. Zhang, X. Li, L. Zhang, C. Shan, *Nano Lett.* **2020**, *20*, 3568.
[122] S. Kumar, J. Jagielski, S. Yakunin, P. Rice, Y.-C. Chiu, M. Wang, G. Nedelcu, Y. Kim, S. Lin, E. J. G. Santos, M. V. Kovalenko, C.-J. Shih, *ACS Nano* **2016**, *10*, 9720.
[123] S. Yuan, Z.-K. Wang, L.-X. Xiao, C.-F. Zhang, S.-Y. Yang, B.-B. Chen, H.-T. Ge, Q.-S. Tian, Y. Jin, L.-S. Liao, *Adv. Mater.* **2019**, *31*, 1904319.
[124] S. Hou, M. K. Gangishetty, Q. Quan, D. N. Congreve, *Joule* **2018**, *2*, 2421.
[125] X. Zheng, S. Yuan, J. Liu, J. Yin, F. Yuan, W.-S. Shen, K. Yao, M. Wei, C. Zhou, K. Song, B.-B. Zhang, Y. Lin, M. N. Hedhili, N. Wehbe, Y. Han, H.-T. Sun, Z.-H. Lu, T. D. Anthopoulos, O. F. Mohammed, E. H. Sargent, L.-S. Liao, O. M. Bakr, *ACS Energy Lett.* **2020**, *5*, 793.
[126] M. Karlsson, Z. Yi, S. Reichert, X. Luo, W. Lin, Z. Zhang, C. Bao, R. Zhang, S. Bai, G. Zheng, P. Teng, L. Duan, Y. Lu, K. Zheng, T. Pullerits, C. Deibel, W. Xu, R. Friend, F. Gao, *Nat. Commun.* **2021**, *12*, 361.
[127] D. Ma, P. Todorović, S. Meshkat, M. I. Saidaminov, Y.-K. Wang, B. Chen, P. Li, B. Scheffel, R. Quintero-Bermudez, J. Z. Fan, Y. Dong, B. Sun, C. Xu, C. Zhou, Y. Hou, X. Li, Y. Kang, O. Voznyy, Z.-H. Lu, D. Ban, E. H. Sargent, *J. Am. Chem. Soc.* **2020**, *142*, 5126.
[128] Y. Dong, Y.-K. Wang, F. Yuan, A. Johnston, Y. Liu, D. Ma, M.-J. Choi, B. Chen, M. Chekini, S.-W. Baek, L. K. Sagar, J. Fan, Y. Hou, M. Wu, S. Lee, B. Sun, S. Hoogland, R. Quintero-Bermudez, H. Ebe, P. Todorovic, F. Dinic, P. Li, H. T. Kung, M. I. Saidaminov, E. Kumacheva, E. Spiecker, L.-S. Liao, O. Voznyy, Z.-H. Lu, E. H. Sargent, *Nat. Nanotechnol.* **2020**, *15*, 668.
[129] Z. Li, Z. Chen, Y. Yang, Q. Xue, H.-L. Yip, Y. Cao, *Nat. Commun.* **2019**, *10*, 1027.
[130] Y. Liu, J. Cui, K. Du, H. Tian, Z. He, Q. Zhou, Z. Yang, Y. Deng, D. Chen, X. Zuo, Y. Ren, L. Wang, H. Zhu, B. Zhao, D. Di, J. Wang, R. H. Friend, Y. Jin, *Nat. Photonics* **2019**, *13*, 760.
[131] F. Yuan, C. Ran, L. Zhang, H. Dong, B. Jiao, X. Hou, J. Li, Z. Wu, *ACS Energy Lett.* **2020**, *5*, 1062.
[132] Q. Wang, X. Wang, Z. Yang, N. Zhou, Y. Deng, J. Zhao, X. Xiao, P. Rudd, A. Moran, Y. Yan, J. Huang, *Nat. Commun.* **2019**, *10*, 5633.
[133] M. K. Gangishetty, S. Hou, Q. Quan, D. N. Congreve, *Adv. Mater.* **2018**, *30*, 1706226.
[134] Z. Ren, J. Yu, Z. Qin, J. Wang, J. Sun, C. C. S. Chan, S. Ding, K. Wang, R. Chen, K. S. Wong, X. Lu, W.-J. Yin, W. C. H. Choy, *Adv. Mater.* **2021**, *33*, 2005570.
[135] F. Zhang, B. Cai, J. Song, B. Han, B. Zhang, H. Zeng, *Adv. Funct. Mater.* **2020**, *30*, 2001732.
[136] Z. Chu, Y. Zhao, F. Ma, C.-X. Zhang, H. Deng, F. Gao, Q. Ye, J. Meng, Z. Yin, X. Zhang, J. You, *Nat. Commun.* **2020**, *11*, 4165.
[137] Y. Liu, Z. Li, J. Xu, Y. Dong, B. Chen, S. M. Park, D. Ma, S. Lee, J. E. Huang, S. Teale, O. Voznyy, E. H. Sargent, *J. Am. Chem. Soc.* **2022**, *144*, 4009.
[138] Y. Liu, L. Cai, Y. Xu, J. Li, Y. Qin, T. Song, L. Wang, Y. Li, L. K. Ono, Y. Qi, B. Sun, *Nano Energy* **2020**, *78*, 105134.
[139] L.-P. Cheng, J.-S. Huang, Y. Shen, G.-P. Li, X.-K. Liu, W. Li, Y.-H. Wang, Y.-Q. Li, Y. Jiang, F. Gao, C.-S. Lee, J.-X. Tang, *Adv. Opt. Mater.* **2019**, *7*, 1801534.
[140] M. Ban, Y. Zou, J. P. H. Rivett, Y. Yang, T. H. Thomas, Y. Tan, T. Song, X. Gao, D. Credgington, F. Deschler, H. Sirringhaus, B. Sun, *Nat. Commun.* **2018**, *9*, 3892.
[141] L. Xu, J. Li, B. Cai, J. Song, F. Zhang, T. Fang, H. Zeng, *Nat. Commun.* **2020**, *11*, 3902.
[142] H. Wang, X. Zhang, Q. Wu, F. Cao, D. Yang, Y. Shang, Z. Ning, W. Zhang, W. Zheng, Y. Yan, S. V. Kershaw, L. Zhang, A. L. Rogach, X. Yang, *Nat. Commun.* **2019**, *10*, 665.
[143] J. Song, T. Fang, J. Li, L. Xu, F. Zhang, B. Han, Q. Shan, H. Zeng, *Adv. Mater.* **2018**, *30*, 1805409.
[144] C. Wu, T. Wu, Y. Yang, J. A. McLeod, Y. Wang, Y. Zou, T. Zhai, J. Li, M. Ban, T. Song, X. Gao, S. Duhm, H. Sirringhaus, B. Sun, *ACS Nano* **2019**, *13*, 1645.
[145] T. Wu, J. Li, Y. Zou, H. Xu, K. Wen, S. Wan, S. Bai, T. Song, J. A. McLeod, S. Duhm, F. Gao, B. Sun, *Angew. Chem., Int. Ed.* **2020**, *59*, 4099.
[146] L. Zhang, X. Yang, Q. Jiang, P. Wang, Z. Yin, X. Zhang, H. Tan, Y. Yang, M. Wei, B. R. Sutherland, E. H. Sargent, J. You, *Nat. Commun.* **2017**, *8*, 15640.
[147] G. Li, J. Huang, H. Zhu, Y. Li, J.-X. Tang, Y. Jiang, *Chem. Mater.* **2018**, *30*, 6099.
[148] C. Zou, Y. Liu, D. S. Ginger, L. Y. Lin, *ACS Nano* **2020**, *14*, 6076.
[149] K. Sim, T. Jun, J. Bang, H. Kamioka, J. Kim, H. Hiramatsu, H. Hosono, *Appl. Phys. Rev.* **2019**, *6*, 031402.
[150] F. Yan, J. Xing, G. Xing, L. Quan, S. T. Tan, J. Zhao, R. Su, L. Zhang, S. Chen, Y. Zhao, A. Huan, E. H. Sargent, Q. Xiong, H. V. Demir, *Nano Lett.* **2018**, *18*, 3157.
[151] C. Wu, Y. Zou, T. Wu, M. Ban, V. Pecunia, Y. Han, Q. Liu, T. Song, S. Duhm, B. Sun, *Adv. Funct. Mater.* **2017**, *27*, 1700338.
[152] Y. Jiang, M. Cui, S. Li, C. Sun, Y. Huang, J. Wei, L. Zhang, M. Lv, C. Qin, Y. Liu, M. Yuan, *Nat. Commun.* **2021**, *12*, 336.
[153] W. Feng, Y. Zhao, K. Lin, J. Lu, Y. Liang, K. Liu, L. Xie, C. Tian, T. Lyu, Z. Wei, *Adv. Funct. Mater.* **2022**, *32*, 2203371.
[154] D. Han, M. Imran, M. Zhang, S. Chang, X.-G. Wu, X. Zhang, J. Tang, M. Wang, S. Ali, X. Li, G. Yu, J. Han, L. Wang, B. Zou, H. Zhong, *ACS Nano* **2018**, *12*, 8808.

[155] D. Zhang, Y. Fu, H. Zhan, C. Zhao, X. Gao, C. Qin, L. Wang, *Light: Sci. Appl.* **2022**, *11*, 69.
[156] C. Zhao, W. Wu, H. Zhan, W. Yuan, H. Li, D. Zhang, D. Wang, Y. Cheng, S. Shao, C. Qin, L. Wang, *Angew. Chem., Int. Ed.* **2022**, *61*, e202117374.
[157] Y.-H. Kim, S. Kim, A. Kakekhani, J. Park, J. Park, Y.-H. Lee, H. Xu, S. Nagane, R. B. Wexler, D.-H. Kim, S. H. Jo, L. Martínez-Sarti, P. Tan, A. Sadhanala, G.-S. Park, Y.-W. Kim, B. Hu, H. J. Bolink, S. Yoo, R. H. Friend, A. M. Rappe, T.-W. Lee, *Nat. Photonics* **2021**, *15*, 148.
[158] X. Yang, X. Zhang, J. Deng, Z. Chu, Q. Jiang, J. Meng, P. Wang, L. Zhang, Z. Yin, J. You, *Nat. Commun.* **2018**, *9*, 570.
[159] X. Yang, Z. Chu, J. Meng, Z. Yin, X. Zhang, J. Deng, J. You, *J. Phys. Chem. Lett.* **2019**, *10*, 2892.
[160] M.-H. Park, J. Park, J. Lee, H. Seob So, H. Kim, S.-H. Jeong, T.-H. Han, C. Wolf, H. Lee, S. Yoo, T.-W. Lee, *Adv. Funct. Mater.* **2019**, *29*, 1902017.
[161] F. Yuan, X. Zhang, A. Johnston, Y.-K. Wang, C. Zhou, Y. Dong, B. Chen, H. Chen, J. Z. Fan, G. Sharma, P. Li, Y. Gao, O. Voznyy, H.-T. Kung, Z.-H. Lu, O. M. Bark, E. H. Sargent, *Sci. Adv.* **2020**, *6*, eabb0253.
[162] Y. Hassan, J. H. Park, M. L. Crawford, A. Sadhanala, J. Lee, J. C. Sadighian, E. Mosconi, R. Shivanna, E. Radicchi, M. Jeong, C. Yang, H. Choi, S. H. Park, M. H. Song, F. D. Angelis, C. Y. Wong, R. H. Friend, B. R. Lee, H. J. Snaith, *Nature* **2021**, *591*, 72.
[163] Y.-K. Wang, F. Yuan, Y. Dong, J.-Y. Li, A. Johnston, B. Chen, M. I. Saidaminov, C. Zhou, X. Zheng, Y. Hou, K. Bertens, H. Ebe, D. Ma, Z. Deng, S. Yuan, R. Chen, L. K. Sagar, J. Liu, J. Fan, P. Li, X. Li, Y. Gao, M.-K. Fung, Z.-H. Lu, O. M. Bakr, L.-S. Liao, E. H. Sargent, *Angew. Chem., Int. Ed.* **2021**, *60*, 16164.
[164] X. Zhang, C. Sun, Y. Zhang, H. Wu, C. Ji, Y. Chuai, P. Wang, S. Wen, C. Zhang, W. W. Yu, *J. Phys. Chem. Lett.* **2016**, *7*, 4602.
[165] D. Zhang, L. Chao, G. Jin, Z. Xing, W. Hong, Y. Chen, L. Wang, J. Chen, D. Ma, *Adv. Funct. Mater.* **2022**, *32*, 2205707.
[166] Y.-K. Wang, K. Singh, J.-Y. Li, Y. Dong, X.-Q. Wang, J. M. Pina, Y.-J. Yu, R. Sabatini, Y. Liu, D. Ma, J. Liu, Z. Liu, Y. Gao, O. Voznyy, W. Ma, M.-K. Fung, L.-S. Liao, E. H. Sargent, *Adv. Mater.* **2022**, *34*, 2200854.
[167] N. Li, S. Apergi, C. C. S. Chan, Y. Jia, F. Xie, Q. Liang, G. Li, K. S. Wong, G. Brocks, S. Tao, N. Zhao, *Adv. Mater.* **2022**, *34*, 2202042.
[168] C. Chen, T. Xuan, Y. Yang, F. Huang, T. Zhou, L. Wang, R.-J. Xie, *ACS Appl. Mater. Interfaces* **2022**, *14*, 16404.
[169] M. Lu, J. Guo, S. Sun, P. Lu, X. Zhang, Z. Shi, W. W. Yu, Y. Zhang, *Chem. Eng. J.* **2021**, *404*, 126563.
[170] X. Shen, Y. Zhang, S. V. Kershaw, T. Li, C. Wang, X. Zhang, W. Wang, D. Li, Y. Wang, M. Lu, L. Zhang, C. Sun, D. Zhao, G. Qin, X. Bai, W. W. Yu, A. L. Rogach, *Nano Lett.* **2019**, *19*, 1552.
[171] M. Lu, J. Guo, S. Sun, P. Lu, J. Wu, Y. Wang, S. V. Kershaw, W. W. Yu, A. L. Rogach, Y. Zhang, *Nano Lett.* **2020**, *20*, 2829.
[172] G. Cheng, Y. Liu, T. Chen, W. Chen, Z. Fang, J. Zhang, L. Ding, X. Li, T. Shi, Z. Xiao, *ACS Appl. Mater. Interfaces* **2020**, *12*, 18084.
[173] M. Lu, X. Zhang, Y. Zhang, J. Guo, X. Shen, W. W. Yu, A. L. Rogach, *Adv. Mater.* **2018**, *30*, 1804691.
[174] X. Zhang, M. Lu, Y. Zhang, H. Wu, X. Shen, W. Zhang, W. Zheng, V. L. Colvin, W. W. Yu, *ACS Cent. Sci.* **2018**, *4*, 1352.
[175] Z. Fang, W. Chen, Y. Shi, J. Zhao, S. Chu, J. Zhang, Z. Xiao, *Adv. Funct. Mater.* **2020**, *30*, 1909754.
[176] X. Zhang, D. Han, C. Wang, I. Muhammad, F. Zhang, A. Shmshad, X. Xue, W. Ji, S. Chang, H. Zhong, *Adv. Opt. Mater.* **2019**, *7*, 1900774.
[177] N. K. Kumawat, A. Dey, A. Kumar, S. P. Gopinathan, K. L. Narasimhan, D. Kabra, *ACS Appl. Mater. Interfaces* **2015**, *7*, 13119.
[178] W. Chen, Y. Shi, J. Chen, P. Ma, Z. Fang, D. Ye, Y. Lu, Y. Yuan, J. Zhao, Z. Xiao, *Adv. Mater.* **2021**, *33*, 2104842.
[179] S.-Y. Chou, R. Ma, Y. Li, F. Zhao, K. Tong, Z. Yu, Q. Pei, *ACS Nano* **2017**, *11*, 11368.
[180] S. G. Bade, X. Shan, P. T. Hoang, J. Li, T. Geske, L. Cai, Q. Pei, C. Wang, Z. Yu, *Adv. Mater.* **2017**, *29*, 1607053.
[181] F. Zhao, D. Chen, S. Chang, H. Huang, K. Tong, C. Xiao, S. Chou, H. Zhong, Q. Pei, *J. Mater. Chem. C* **2017**, *5*, 531.
[182] H.-K. Seo, H. Kim, J. Lee, M.-H. Park, S.-H. Jeong, Y.-H. Kim, S.-J. Kwon, T.-H. Han, S. Yoo, T.-W. Lee, *Adv. Mater.* **2017**, *29*, 1605587.
[183] H. Rui, L. Li, N. Zhang, X. Lin, Y. Hua, X. Wu, D. Wang, S. Yin, *IEEE Electron Device Lett.* **2018**, *40*, 59.
[184] L. Zhao, N. Rolston, K. M. Lee, X. Zhao, M. A. Reyes-Martinez, N. L. Tran, Y.-W. Yeh, N. Yao, G. D. Scholes, Y.-L. Loo, A. Selloni, R. H. Dauskardt, B. P. Rand, *Adv. Funct. Mater.* **2018**, *28*, 1802060.
[185] Y.-S. Liu, S. Guo, F.-S. Yi, J. Feng, H.-B. Sun, *Opt. Lett.* **2018**, *43*, 5524.
[186] D. H. Jung, J. H. Park, H. E. Lee, J. Byun, T. H. Im, G. Y. Lee, J. Y. Seok, T. Yun, K. J. Lee, S. O. Kim, *Nano Energy* **2019**, *61*, 236.
[187] J. Li, P. Du, S. Li, J. Liu, M. Zhu, Z. Tan, M. Hu, J. Luo, D. Guo, L. Ma, Z. Nie, Y. Ma, L. Gao, G. Niu, J. Tang, *Adv. Funct. Mater.* **2019**, *29*, 1903607.
[188] Y. Li, S. Chou, P. Huang, C. Xiao, X. Liu, Y. Xie, F. Zhao, Y. Huang, J. Feng, H. Zhong, H. Sun, Q. Pei, *Adv. Mater.* **2019**, *31*, 1807516.
[189] S. Y. Lee, Y. S. Nam, J. C. Yu, S. Lee, E. D. Jung, S.-H. Kim, S. Lee, J.-Y. Kim, M. H. Song, *ACS Appl. Mater. Interfaces* **2019**, *11*, 39274.
[190] M. Lu, H. Wu, X. Zhang, H. Wang, Y. Hu, V. L. Colvin, Y. Zhang, W. W. Yu, *ChemNanoMat* **2019**, *5*, 313.
[191] M. Payandeh, V. Ahmadi, F. A. Roghabadi, P. Nazari, F. Ansari, P. Brenner, R. Bauerle, M. Jakoby, U. Lemmer, I. A. Howard, B. S. Richards, U. W. Paetzold, B. A. Nejand, *ACS Appl. Mater. Interfaces* **2020**, *12*, 11428.
[192] X. Zhao, Z.-K. Tan, *Nat. Photonics* **2020**, *14*, 215.
[193] H. Kang, S.-R. Choi, Y.-H. Kim, J. S. Kim, S. Kim, B.-S. An, C.-W. Yang, J.-M. Myoung, T.-W. Lee, J.-G. Kim, J. H. Cho, *ACS Appl. Mater. Interfaces* **2020**, *12*, 39479.
[194] Y. Shen, M.-N. Li, Y. Li, F.-M. Xie, H.-Y. Wu, G.-H. Zhang, L. Chen, S.-T. Lee, J.-X. Tang, *ACS Nano* **2020**, *14*, 6107.
[195] C. Chen, T.-H. Han, S. Tan, J. Xue, Y. Zhao, Y. Liu, H. Wang, W. Hu, C. Bao, M. Mazzeo, R. Wang, Y. Duan, Y. Yang, *Nano Lett.* **2020**, *20*, 4673.
[196] Y. Liu, L. Zhang, S. Chen, C. Liu, Y. Li, J. Wu, D. Wang, Z. Jiang, Y. Li, Y. Li, X. Wang, B. Xu, *Small* **2021**, *17*, 2101477.
[197] Y. Liu, Z. Yu, S. Chen, J. H. Park, E. D. Jung, S. Lee, K. Kang, S.-J. Ko, J. Lim, M. H. Song, B. Xu, H. J. Snaith, S. H. Park, B. R. Lee, *Nano Energy* **2021**, *80*, 105511.
[198] P. Du, J. Li, L. Wang, L. Sun, X. Wang, X. Xu, L. Yang, J. Pang, W. Liang, J. Luo, Y. Ma, J. Tang, *Nat. Commun.* **2021**, *12*, 4751.
[199] S. Chu, W. Chen, Z. Fang, X. Xiao, Y. Liu, J. Chen, J. Huang, Z. Xiao, *Nat. Commun.* **2021**, *12*, 147.
[200] F. Cao, M. You, L. Kong, Y. Dou, Q. Wu, L. Wang, B. Wei, X. Zhang, W.-Y. Wong, X. Yang, *Nano Lett.* **2022**, *22*, 4246.
[201] J. I. Kwon, G. Park, G. H. Lee, J. H. Jang, N. J. Sung, S. Y. Kim, J. Yoo, K. Lee, H. Ma, M. Karl, T. J. Shin, M. H. Song, J. Yang, M. K. Choi, *Sci. Adv.* **2022**, *8*, eadd0697.
[202] J. K. Park, S. Y. Kim, J. H. Kim, J. H. Heo, S. H. Im, *J. Alloys Compd.* **2022**, *918*, 165560.
[203] D.-H. Jiang, Y.-C. Liao, C.-J. Cho, L. Veeramuthu, F.-C. Liang, T.-C. Wang, C.-C. Chueh, T. Satoh, S.-H. Tung, C.-C. Kuo, *ACS Appl. Mater. Interfaces* **2020**, *12*, 14408.
[204] S. Benhouhou, A. Mekki, M. Ayat, N. Gabouze, *Macromol. Res.* **2021**, *29*, 267.
[205] J. Zhao, L.-W. Lo, H. Wan, P. Mao, Z. Yu, C. Wang, *Adv. Mater.* **2021**, *33*, 2102095.
[206] S. W. Jin, Y. H. Lee, K. M. Yeom, J. Yun, H. Park, Y. R. Jeong, S. Y. Hong, G. Lee, S. Y. Oh, J. H. Lee, J. H. Noh, J. S. Ha, *ACS Appl. Mater. Interfaces* **2018**, *10*, 30706.
[207] C. Park, M. S. Kim, H. H. Kim, S.-H. Sunwoo, D. J. Jung, M. K. Choi, D.-H. Kim, *Appl. Phys. Rev.* **2022**, *9*, 021312.

[208] D. C. Kim, H. J. Shim, W. Lee, J. H. Kim, D.-H. Kim, *Adv. Mater.* **2020**, *32*, 1902743.
[209] J.-K. Song, J. Kim, J. Yoon, J. H. Koo, H. Jung, K. Kang, S.-H. Sunwoo, S. Yoo, H. Chang, J. Jo, W. Baek, S. Lee, M. Lee, H. J. Kim, M. Shin, Y. J. Yoo, Y. M. Song, T. Hyeon, D.-H. Kim, D. Son, *Nat. Nanotechnol.* **2022**, *17*, 849.
[210] D. Jung, C. Lim, H. J. Shim, Y. Kim, C. Park, J. Jung, S. I. Han, S.-H. Sunwoo, K. W. Cho, G. D. Cha, D. C. Kim, J. H. Koo, J. H. Kim, T. Hyeon, D.-H. Kim, *Science* **2021**, *373*, 1022.
[211] S. Choi, S. I. Han, D. Jung, H. J. Hwang, C. Lim, S. Bae, O. K. Park, C. M. Tschabrunn, M. Lee, S. Y. Bae, J. W. Yu, J. H. Ryu, S.-W. Lee, K. Park, P. M. Kang, W. B. Lee, R. Nezafat, T. Hyeon, D.-H. Kim, *Nat. Nanotechnol.* **2018**, *13*, 1048.
[212] Y. U. Kim, S. H. Park, N. T. Nhan, M. H. Hoang, M. J. Cho, D. H. Choi, *Macromol. Res.* **2021**, *29*, 75.
[213] C. Wu, F. Li, W. Wu, W. Chen, T. Guo, *Appl. Phys. Lett.* **2014**, *105*, 243509.
[214] H. Jang, K. Sel, E. Kim, S. Kim, X. Yang, S. Kang, K.-H. Ha, R. Wang, Y. Rao, R. Jafari, N. Lu, *Nat. Commun.* **2022**, *13*, 2739.
[215] M. Vosgueritchian, D. J. Lipomi, Z. Bao, *Adv. Funct. Mater.* **2012**, *22*, 421.
[216] S.-H. Jeong, S.-H. Woo, T.-H. Han, M.-H. Park, H. Cho, Y.-H. Kim, H. Cho, H. Kim, S. Yoo, T.-W. Lee, *NPG Asia Mater.* **2017**, *9*, e411.
[217] P. Lee, J. Lee, H. Lee, J. Yeo, S. Hong, K. H. Nam, D. Lee, S. S. Lee, S. H. Ko, *Adv. Mater.* **2012**, *24*, 3326.
[218] K. Hantanasirisakul, M.-Q. Zhao, P. Urbankowski, J. Halim, B. Anasori, S. Kota, C. E. Ren, M. W. Barsoum, Y. Gogotsi, *Adv. Electron. Mater.* **2016**, *2*, 1600050.
[219] D. C. Kim, H. Yun, J. Kim, H. Seung, W. S. Yu, J. H. Koo, J. Yang, J. H. Kim, T. Hyeon, D.-H. Kim, *Nat. Electron.* **2021**, *4*, 671.
[220] H.-C. Wang, Z. Bao, H.-Y. Tsai, A. C. Tang, R.-S. Liu, *Small* **2018**, *14*, 1702433.
[221] Y. Guo, Y. Jia, N. Li, M. Chen, S. Hu, C. Liu, N. Zhao, *Adv. Funct. Mater.* **2020**, *30*, 1910464.
[222] K. H. Park, D. B. Kim, D. E. Lee, K. S. Park, Y. S. Cho, *J. Alloys Compd.* **2022**, *908*, 164607.
[223] D. Yu, Y.-Q. Yang, Z. Chen, Y. Teo, Y.-F. Liu, *Opt. Commun.* **2016**, *362*, 43.
[224] W. Lee, J. Lee, H. Yun, J. Kim, J. Park, C. Choi, D. C. Kim, H. Seo, H. Lee, J. W. Yu, W. B. Lee, D.-H. Kim, *Adv. Mater.* **2017**, *29*, 1702902.
[225] J. Park, H. Seung, D. C. Kim, M. S. Kim, D.-H. Kim, *Adv. Funct. Mater.* **2021**, *31*, 2009281.
[226] D. Zhang, Q. Zhang, E. Ren, Y. Zhu, M. Abdellah, Y. Fu, B. Cao, C. Wang, L. Gu, Y. Ding, K.-H. Tsui, S. Fan, S. Poddar, L. Sho, Y. Zhang, D.-B. Kuang, J.-F. Liao, Y. Lu, K. Zheng, Z. He, Z. Fan, *Nat. Photonics* **2022**, *16*, 284.
[227] J. Yoo, S. Li, D.-H. Kim, J. Yang, M. K. Choi, *Nanoscale Horiz.* **2022**, *7*, 801.
[228] M. Ha, S. Lim, H. Ko, *J. Mater. Chem. B* **2018**, *6*, 4043.
[229] T. Yokota, P. Zalar, M. Kaltenbrunner, H. Jinno, N. Matsuhisa, H. Kitanosako, Y. Tachibana, W. Yukita, M. Koizumi, T. Someya, *Sci. Adv.* **2016**, *2*, e1501856.
[230] S. Y. Kim, J. I. Kwon, H. H. Song, G. H. Lee, W. S. Yu, S. Li, M. K. Choi, J. Yang, *Appl. Surf. Sci.* **2023**, *610*, 155579.
[231] J. Yang, J. Yoo, W. S. Yu, M. K. Choi, *Macromol. Res.* **2021**, *29*, 391.
[232] Y. Lee, Y. J. Han, K. Y. Cho, K. H. Cho, Y.-C. Jeong, *Macromol. Res.* **2021**, *29*, 172.

Jae Hong Jang received his B.S. (2020) degree from the Department of Materials Science and Engineering at Ulsan National Institute of Science and Technology (UNIST). Under the supervision of Prof. Moon Kee Choi, he is working on the fabrication and application of wearable optoelectronic devices (light-emitting diodes and photodetectors) for his Ph.D. study.

Shi Li received her B.E. (2017) degree from the School of Engineering at Lishui University of China and her M.E. (2020) degree from the School of Science at Zhejiang Sci-Tech University of China. She is now pursuing her Ph.D. degree in the Department of Energy Science and Engineering under the supervision of Prof. Jiwoong Yang at Daegu Gyeongbuk Institute of Science and Technology (DGIST). Her recent research focuses on the fabrication of high-performance optoelectronic devices using semiconductor nanocrystals.

Dae-Hyeong Kim is a professor in the School of Chemical and Biological Engineering at Seoul National University, an associate director of Center for Nanoparticle Research of Institute for Basic Science (IBS), and an associate editor of Science Advances. He received his B.S. (2000) and M.S. (2002) degrees from the School of Chemical Engineering at Seoul National University. He obtained his Ph.D. (2009) from the Department of Materials Science and Engineering at the University of Illinois at Urbana–Champaign. Since he joined at Seoul National University in 2011, he has focused on stretchable and soft electronics for biomedical and energy applications.

Jiwoong Yang is an assistant professor in the Department of Energy Science and Engineering of Daegu Gyeongbuk Institute of Science and Technology (DGIST). He received his B.S. (2011) and Ph.D. (2016) in chemical and biological engineering from Seoul National University under the guidance of Prof. Taeghwan Hyeon. He conducted his postdoctoral research at Lawrence Berkeley National Laboratory under the supervision of Dr. Haimei Zheng. His research interests include synthesis and characterization of inorganic nanocrystals for energy and electronic devices.

Moon Kee Choi is an associate professor in the Department of Materials Science and Engineering of Ulsan National Institute of Science and Technology (UNIST). She received her B.S. (2009) and Ph.D. (2016) in chemical and biological engineering from Seoul National University under the guidance of Prof. Dae-Hyeong Kim. She conducted her postdoctoral research at UC Berkeley under the supervision of Prof. Seung-Wuk Lee. Now, she is focusing on the development of next-generation optoelectronic-devices, biomedical electronics, and soft robotics with deformable form factors.